

See discussions, stats, and author profiles for this publication at: <https://www.researchgate.net/publication/318991130>

A mangrove forest map of China in 2015: Analysis of time series Landsat 7/8 and Sentinel-1A imagery in Google Earth Engine cloud computing platform

Article in ISPRS Journal of Photogrammetry and Remote Sensing · August 2017

DOI: 10.1016/j.isprsjprs.2017.07.011

CITATIONS

135

READS

3,759

15 authors, including:



Bangqian Chen
Chinese Academy of Tropical Agricultural Sciences/Fudan university

42 PUBLICATIONS 895 CITATIONS

[SEE PROFILE](#)



Xiangming Xiao
University of Oklahoma

357 PUBLICATIONS 16,406 CITATIONS

[SEE PROFILE](#)



Pan Lianghai
Fudan University

13 PUBLICATIONS 183 CITATIONS

[SEE PROFILE](#)



Russell Doughty
California Institute of Technology

62 PUBLICATIONS 1,041 CITATIONS

[SEE PROFILE](#)

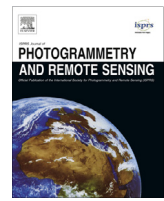
Some of the authors of this publication are also working on these related projects:



Great Plains Grazing [View project](#)



Global vegetation productivity simulation [View project](#)



A mangrove forest map of China in 2015: Analysis of time series Landsat 7/8 and Sentinel-1A imagery in Google Earth Engine cloud computing platform



Bangqian Chen^{a,b}, Xiangming Xiao^{b,c,*}, Xiangping Li^b, Lianghao Pan^{b,d}, Russell Doughty^c, Jun Ma^b, Jinwei Dong^c, Yuanwei Qin^c, Bin Zhao^b, Zhixiang Wu^a, Rui Sun^a, Guoyu Lan^a, Guishui Xie^a, Nicholas Clinton^e, Chandra Giri^f

^aRubber Research Institute (RRI), Chinese Academy of Tropical Agricultural Sciences, Danzhou City (CATAS); Danzhou Investigation & Experiment Station of Tropical Crops, Ministry of Agriculture, Hainan Province 571737, PR China

^bMinistry of Education Key Laboratory for Biodiversity Science and Ecological Engineering, Institute of Biodiversity Sciences, Fudan University, Shanghai 200438, PR China

^cDepartment of Microbiology and Plant Biology, and Center for Spatial Analysis, University of Oklahoma, Norman, OK 73019, USA

^dGuangxi Key Lab of Mangrove Conservation and Utilization, Guangxi Mangrove Research Center (GMRC), Guangxi Academy of Sciences, Beihai, Guangxi Zhuang Autonomous Region 536000, PR China

^eGoogle, Mountain View, CA, USA

^fSensing and Spatial Analysis Branch, U. S. Environmental Protection Agency, Research Triangle Park, NC 27709, USA

ARTICLE INFO

Article history:

Received 28 March 2017

Received in revised form 20 July 2017

Accepted 28 July 2017

Keywords:

ETM+/OLI

SAR

NDVI

Greenness

Canopy coverage

Tidal inundation

ABSTRACT

Due to rapid losses of mangrove forests caused by anthropogenic disturbances and climate change, accurate and contemporary maps of mangrove forests are needed to understand how mangrove ecosystems are changing and establish plans for sustainable management. In this study, a new classification algorithm was developed using the biophysical characteristics of mangrove forests in China. More specifically, these forests were mapped by identifying: (1) greenness, canopy coverage, and tidal inundation from time series Landsat data, and (2) elevation, slope, and intersection-with-sea criterion. The annual mean Normalized Difference Vegetation Index (NDVI) was found to be a key variable in determining the classification thresholds of greenness, canopy coverage, and tidal inundation of mangrove forests, which are greatly affected by tide dynamics. In addition, the integration of Sentinel-1A VH band and modified Normalized Difference Water Index (mNDWI) shows great potential in identifying yearlong tidal and fresh water bodies, which is related to mangrove forests. This algorithm was developed using 6 typical Regions of Interest (ROIs) as algorithm training and was run on the Google Earth Engine (GEE) cloud computing platform to process 1941 Landsat images (25 Path/Row) and 586 Sentinel-1A images circa 2015. The resultant mangrove forest map of China at 30 m spatial resolution has an overall/users/producer's accuracy greater than 95% when validated with ground reference data. In 2015, China's mangrove forests had a total area of 20,303 ha, about 92% of which was in the Guangxi Zhuang Autonomous Region, Guangdong, and Hainan Provinces. This study has demonstrated the potential of using the GEE platform, time series Landsat and Sentinel-1A SAR images to identify and map mangrove forests along the coastal zones. The resultant mangrove forest maps are likely to be useful for the sustainable management and ecological assessments of mangrove forests in China.

© 2017 International Society for Photogrammetry and Remote Sensing, Inc. (ISPRS). Published by Elsevier B.V. All rights reserved.

1. Introduction

Mangrove forests are tidal wetlands with a diverse assemblage of trees and shrubs and are located in the tropical and subtropical

* Corresponding author at: Department of Microbiology and Plant Biology, and Center for Spatial Analysis, University of Oklahoma, Norman, OK 73019, USA.

E-mail addresses: chbq40@163.com (B. Chen), xiangming.xiao@ou.edu (X. Xiao).

regions between approximately 30°N and 30°S latitude (Lee and Yeh, 2009; Giri et al., 2011). These forests provide a wide range of ecosystem services such as nursery habitats for many marine fisheries, water purification, shoreline stabilization, biological diversity, and are important to the recreation and tourism industry (Rahman et al., 2013; Abdul Aziz et al., 2015; Giri et al., 2015). Mangrove forests are among the most carbon-rich forests in the tropics, which make them important areas for study due to current

losses in forest cover and ecosystem degradation. These forests are candidates for conservation efforts under schemes such as Reduce Emission from Deforestation and Degradation (REDD+) (Donato et al., 2011; Kirui et al., 2013). The mangrove forest ecosystem is one of the most vulnerable ecosystems on Earth due to anthropogenic disturbance and climate change (e.g. Sea level rise). It has been reported that 20–35% of global mangrove forest lands have been lost due to deforestation since the 1980s (FAO, 2007; Rahman et al., 2013). The rapid loss of mangrove forests is compelling managers and scientists to inventory and monitor their spatial extent, and a considerable number of monitoring efforts have been conducted from the local to global scales (Giri et al., 2008, 2011, 2015; Spalding et al., 2010; Kirui et al., 2013; McCarthy et al., 2015; Hamilton and Casey, 2016). Two global scale mangrove forest maps were produced for the year 2000: The World Atlas of Mangroves (referred as WAM10) by Spalding et al. (2010), and Mangrove Forests of the World (MFW) by Giri et al. (2011). More recently, Hamilton and Casey (2016) released the Global Database of Continuous Mangrove Forest Cover for the 21st Century (CGMFC-21) from 2000 to 2012 by integrating the Global Forest Cover (GFC) dataset (Hansen et al., 2013), MFW, and the Terrestrial Ecoregions of the World (TEOW) (Olson et al., 2001). Their works have contributed to the studies of mangrove forest biodiversity and carbon stocks and to the efforts for conservation of mangrove forest ecosystems.

However, these aforementioned mangrove forest maps in China are incomplete or outdated, and therefore cannot reflect the latest spatial distribution of mangrove forests in China. For example, only about 14% (3139 ha) of the mangrove forests in China were mapped in the MFW map (Hamilton and Casey, 2016). This incomplete mangrove forest mapping in China was propagated to the annual CGMFC-21 maps since they were generated using the MFW base map of 2000 and annual forest loss map of GFC (2001–2012). Moreover, gains in mangrove forest cover were not considered. The WAM10 included China, but the map is not contemporary because it was generated using Landsat Thematic Mapper (TM) and Enhanced Thematic Mapper (ETM+) data acquired between 1999 and 2003 (Spalding et al., 2010). Therefore, it is critical that the coverage and spatial distribution of mangrove forests in China be accurately mapped using the most recent image data and improved remote sensing techniques.

Table 1 provides a summary on existing data, algorithms, and map products for mangrove forest mapping. Supervised and unsupervised classification methods were used in most of the published studies. These algorithms can generate accurate mangrove forest maps for specific regions at specific time (image acquisition time), but are often difficult to scale-out to larger areas at other times. The majority of the published studies were based on moderate to high spatial resolution optical satellite images such as Landsat data. A few studies were based on integrating optical and Synthetic Aperture Radar (SAR) data, and they demonstrated that optical and SAR data could complement each other by combining spectral and structural information of mangrove forests, thereby overcoming the problems caused by clouds and shadows in optical imagery. Rahman et al. (2013) used time series Moderate Resolution Imaging Spectroradiometer (MODIS) to map mangrove forests, but the other studies often used imagery from a single date or multiple dates. Time series images were rarely used to map mangrove forests.

Time series Landsat data can provide more phenological information for land cover classification, and their advantages have been illustrated in recent studies (Hermosilla et al., 2015; Reiche et al., 2015; Dong et al., 2016; Zhou et al., 2016). Several of those studies analyzed time series spectral data of individual pixels and used the phenology-based spectral signatures to identify and generate maps of forests, rubber plantations, and paddy rice

croplands (Dong et al., 2013, 2016; Kou et al., 2015). With the increasing amount of cost-free time series data from satellites such as Landsat and Sentinel, releasing of batch pre-processing software/tools for cloud detection (e.g., Fmask (Zhu and Curtis, 2012)) and atmospheric correction (e.g., Landsat Ecosystem Disturbance Adaptive Processing System (LEDAPS) (Maiersperger et al., 2013; Masek et al., 2013)), as well as cloud computation resources like Google Earth Engine (GEE, <https://earthengine.google.com>), there exists a great deal of potential in the phenology-based approach to identify and map mangrove forests using time series optical and SAR images.

The objectives of this study were to (1) develop a phenology-based algorithm to identify mangrove forests by analyzing time series Landsat and Sentinel-1A images, and (2) apply the algorithm to generate a mangrove forest map of China in 2015 and evaluate its performance with ground reference data and publicly available maps and data of mangrove forests. China is an ideal region for studying the cold resistance of mangrove forests, the response of mangrove forest to global warming, and the impacts of human activity such as conservation, restoration, population growth, and rapid economic development (Chen et al., 2009). According to the forest census statistics, China has about 22,000 ha of mangrove forests, which have high species-richness and biodiversity (Chen et al., 2009; Spalding et al., 2010). Several studies estimated the mangrove forest area in China from the local (Lee and Yeh, 2009; Wu et al., 2011; Li et al., 2013; Li and Dai, 2014; Zhang et al., 2015; Wang et al., 2016) to national scale (Chen et al., 2009; Spalding et al., 2010; Wu et al., 2013; Jia et al., 2014). However, these estimates were highly variable at the national scale, ranging from 19,788 ha (Spalding et al., 2010) to 24,578 ha (Wu et al., 2013). The total extent of mangrove forests at the province scale also varied widely (Wu et al., 2013; Jia et al., 2014). Because of the extensive distribution of mangrove forests along coastlines and high fragmentation caused by intensive human disturbance, it is a challenging task to accurately map mangrove forests in China.

2. Material and methods

2.1. Study area

The study area included the coastal mangrove ecosystems in southern China (Fig. 1), comprising areas in the Guangxi Zhuang Autonomous Region (referred as Guangxi ZAR), Hong Kong, Macao, Taiwan and the provinces of Guangdong, Hainan, Fujian and Zhejiang. Natural mangrove forests are mainly distributed within latitudes between 18°09'N and 27°20'N, while planted mangrove forests have extended to Leqing Bay in Zhejiang Province with latitude of 28°25'N (Spalding et al., 2010; Wu et al., 2013). Historically, the total area of mangrove forests in China was 250,000 ha, and in 1950s was about 420,000 ha (Liao and Zhang, 2014), and continue to decrease due to extensive land conversion, salt production, aquaculture, and urbanization (Wu et al., 2013). The total area of mangrove forests in 2002 was 22,025 ha, excluding Hong Kong, Macao, and Taiwan (Chen et al., 2009). Predominant plant species are *Bruguiera gymnorhiza*, *Kandelia obovata*, *Avicennia marina*, *Aegiceras corniculatum*, *Acrostichum aureum*, *Acanthus ilicifolius* (Liao and Zhang, 2014).

2.2. Data

2.2.1. Landsat images and preprocessing

Complete coverage of the study area is 25 tiles of the Landsat Worldwide Reference System (WRS) path/rows. A total of 1941 Landsat surface reflectance (SR) images were acquired between

Table 1

A brief summary on image data and algorithms from selected peer-reviewed references related to mangrove forest mapping.

Methods	Optical images			SAR images	Optical + SAR images
	VHSR/HR	MR	CR		
VI			Spalding et al. (2010), Pattanaik and Narendra Prasad (2011), Wu et al. (2013)		
MLC	Lee and Yeh (2009)	Ramírez-García et al. (1998), Krause et al. (2004), Giri et al. (2007), Lee and Yeh (2009), Salami et al. (2010), Kirui et al. (2013)			Held et al. (2003), Rodrigues and Souza-Filho (2011) [#] , Jhonnerie et al. (2015)
Supervised	NN SVM CART/PE/DT	Wang et al. (2016)	Seto and Fragkias (2007) Long and Skewes (1996) [#] , Giri et al. (2015), Almahasheer et al. (2016)		Held et al. (2003)
Unsupervised	RF			Simard et al. (2002)	Jhonnerie et al. (2015)
ISODATA			Simard et al. (2008), Long and Giri (2011), Li et al. (2013), Carney et al. (2014) [#] , Giri et al. (2015)		
Hybrid supervised and unsupervised			Giri et al. (2008, 2011) [#] , Ibharam et al. (2015)		
OO	Vo et al. (2013) [#] , Liu et al. (2014)	Conchedda et al. (2008), Jia et al. (2014) [#]		De Santiago et al. (2013) [#]	
Knowledge-based	Others			Rahman et al. (2013)*	Rocha De Souza Pereira et al. (2012)
Phenology					This study

VHSR: Very high spatial resolution satellite image (e.g., Worldview-3); **HR:** High resolution satellite image (e.g., SPOT); **MR:** Moderate resolution satellite image (e.g., Landsat); **CR:** coarse resolution satellite image (e.g., MODIS); **SAR:** Synthetic Aperture Radar; **VI:** Visual interpretation; **NN:** Neural Network; **SVM:** Support Vector Machine; **CART:** Classification and Regression Tree; **PE:** Parallel-epeid; **RF:** Random forest; **ISODATA:** Iterative Self-Organizing Data Analysis Technique Algorithm; **OO:** Objected oriented; **DT:** Decision Tree; **Others:** User's defined algorithm.

* Indicate time series data were used, the others were based on images of single date or mosaic.

Indicate visual interpretation methods were employed to refine the mangrove forest maps.

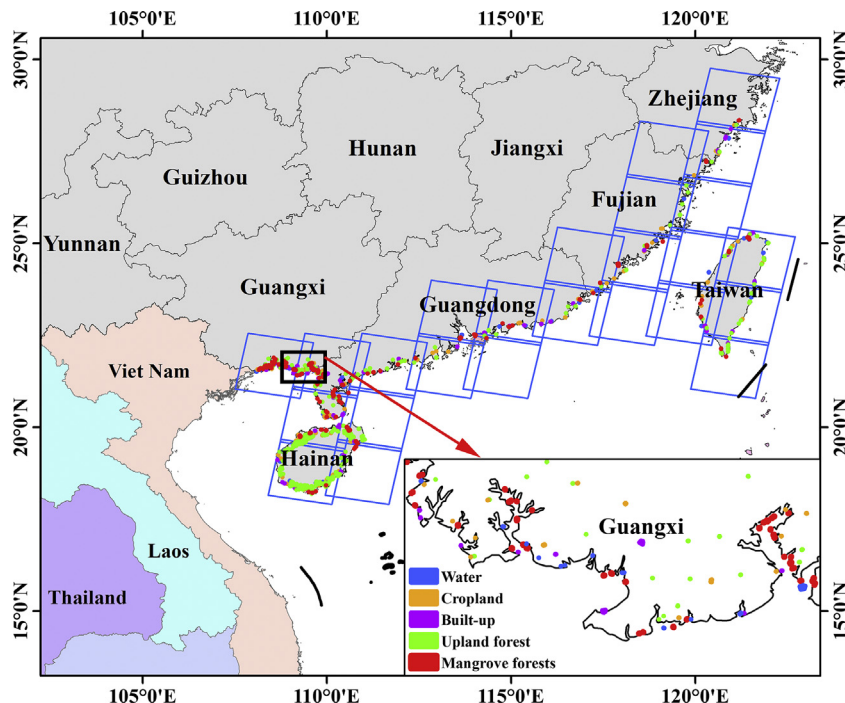


Fig. 1. Location of study area, spatial distribution of Region of Interests (ROIs), and coverage of Landsat Worldwide Reference System 2 (WRS-2) path/row for the study area in Southern China. (For interpretation of the references to color in this figure legend, the reader is referred to the web version of this article.)

January 1, 2014 and July 23, 2016, and were available on GEE as image collections. All Landsat SR data was processed based on standard Level 1 Terrain-corrected (L1T) ortho-rectified images and have high geometric accuracy. The Landsat 8 Operational Land Imager (OLI) SR data was generated by LaSRC software (USGS,

2016), while Landsat 7 ETM + SR data was created by the LEDAPS (Masek et al., 2013; USGS, 2017). Poor quality observations of each Landsat imagery include clouds and shadows identified by *cfmask* band from SR collection and *fmask* band from top-of-atmosphere (TOA) reflectance with Fmask collection (Zhu et al., 2015; USGS,

2016, 2017). Observations unaffected by clouds and shadows, and ETM + scan-line-off strips were considered good quality observation. The spatial distribution of total observations, good quality observations, and percentage of good quality observations for all Landsat images are presented in Fig. 2a–c.

Four widely used vegetation indices such as Nominalized Difference Vegetation Index (NDVI) (Tucker, 1979), Enhanced Vegetation Index (EVI) (Huete et al., 1997, 2002), Land Surface Water Index (LSWI) (Gao, 1996; Xiao et al., 2004), and modified Normalized Difference Water Index (mNDWI) (Xu, 2006) were calculated for each imagery, using Eqs. (1)–(4).

$$NDVI = \frac{\rho_{NIR} - \rho_{red}}{\rho_{NIR} + \rho_{red}} \quad (1)$$

$$EVI = 2.5 \times \frac{\rho_{NIR} - \rho_{red}}{\rho_{NIR} + 6 \times \rho_{red} - 7.5 \times \rho_{blue} + 1} \quad (2)$$

$$LSWI = \frac{\rho_{NIR} - \rho_{SWIR}}{\rho_{NIR} + \rho_{SWIR}} \quad (3)$$

$$mNDWI = \frac{\rho_{green} - \rho_{SWIR}}{\rho_{green} + \rho_{SWIR}} \quad (4)$$

where ρ_{blue} , ρ_{green} , ρ_{red} , ρ_{NIR} , and ρ_{SWIR} are blue (B1:450–520 nm), green (B2:520–600 nm), red (B3:630–690 nm), near-infrared (NIR, B4:760–900 nm), and shortwave infrared (SWIR, B5:1550–1750 nm) bands of Landsat ETM+/OLI imagery, respectively.

2.2.2. Sentinel-1 images and preprocessing

Sentinel-1A carries a C-band imager at 5.405 GHz with incidence angle between 20° and 45° and a 12-day repeat cycle at the equator (Torbick et al., 2016). The Level 1 Ground Range Detected (GRD) product in the Interferometric Wide (IW) swath model, which has dual-polarization of vertical transmitting with vertical receiving (VV) and vertical transmitting with horizontal receiving (VH) bands, was used in this study. Each tile has high geometric accuracy and was processed with Sentinel-1 Toolbox using these steps: (1) thermal noise removal, (2) radiometric calibration, (3) terrain correction (orthorectification) using DEM data from either the Shuttle Radar Topography Mission (SRTM, 30-m, (Farr et al., 2007)) or Advanced Spaceborne Thermal Emission and Reflection Radiometer (ASTER), and 4) conversion of backscatter coefficient (σ^0) to decibels (dB) (Sentinel-1 Team, 2013). The spatial resolution of Sentinel-1A was 10-m and already available in GEE as an image collection. A total of 586 Sentinel-1A images acquired from April 3, 2014 (Lunch date) to July 23, 2016 were

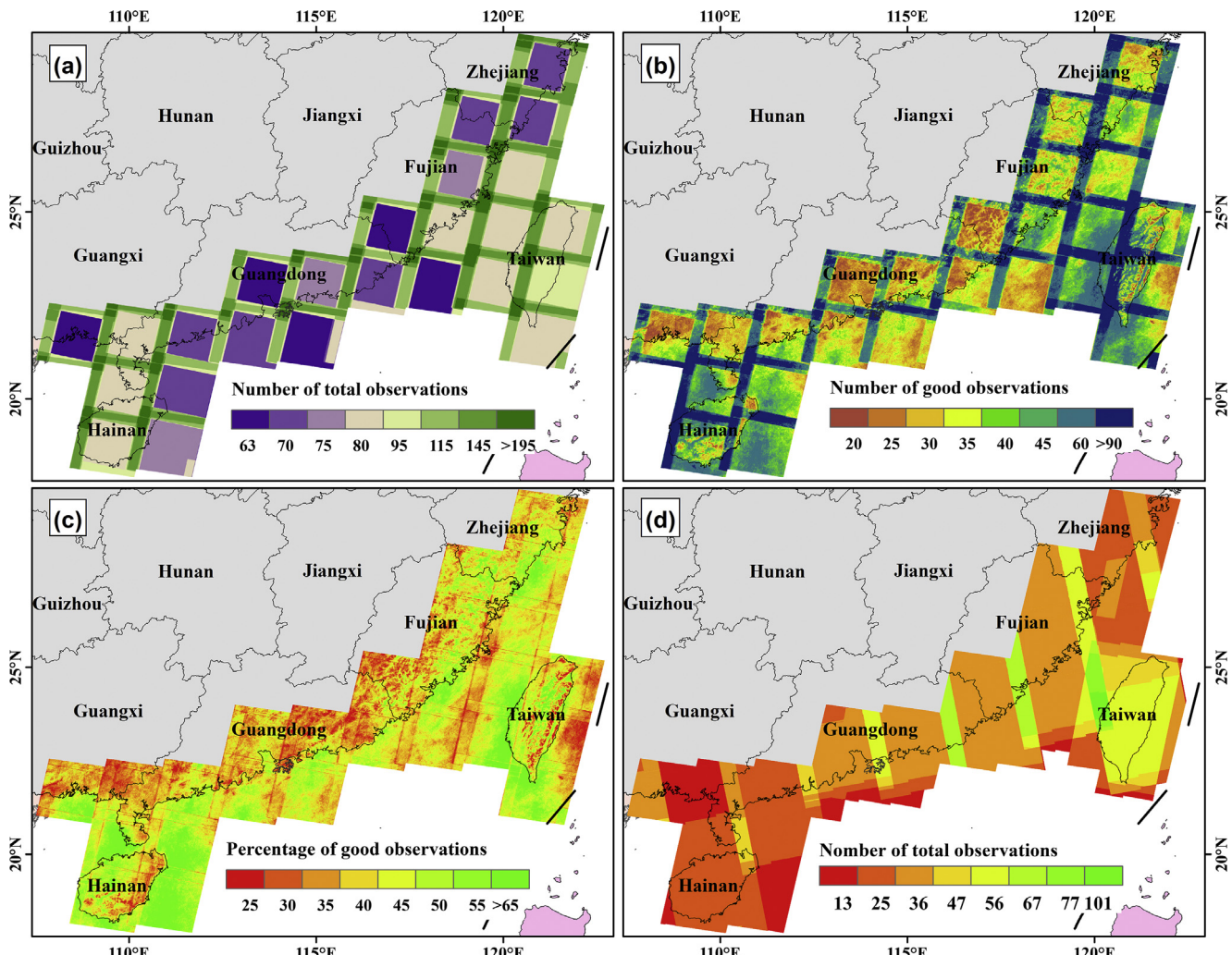


Fig. 2. Spatial distribution of Landsat optical and Sentinel-1A SAR data used in this study: number of (a) total observations and (b) good quality observations for Landsat ETM+/OLI images, (c) percentage of good quality observations for Landsat ETM+/OLI images, and (d) total number of Sentinel-1A SAR images. The number of total/good observations in the four corners of path/row overlapping area are counted four times, while in other path/row overlapping area are counted twice. (For interpretation of the references to color in this figure legend, the reader is referred to the web version of this article.)

used, and the number of total observations was presented in Fig. 2d.

All the Landsat and Sentinel-1A data processing was conducted in GEE. GEE is a cloud-based platform for planetary-scale environmental data analysis. It combines a multi-petabyte catalog of satellite imagery and geospatial datasets, Google's computational infrastructure optimized for parallel processing of geospatial data, Application Programming Interfaces (APIs) for JavaScript and Python, and a web-based integrated development environment for rapid prototyping and visualization of complex spatial analyses. GEE is designed so that users rarely have to worry about map projections when doing computing at large area, projection parameters are requested in the output projection. By default, GEE performs nearest neighbor (NN) resampling during reprojection.

2.2.3. DEM and vector maps

The 30-m SRTM DEM data and their derived variable (slope) were used to mask out those regions of high elevation and/or steep-slope where mangrove forests are not likely to occur. The administrative boundary map of China (Shapefile format, 1: 10,000,000 scale) was used to delineate the coastline. The vector map of Mangrove Forests in South Asia in 2015 (referred as MFSA15), which was produced by Lü et al. (2015) using Landsat 8 images acquired between 2013 and 2015, was downloaded from the Global Change Research Data Publishing & Repository website. In addition, the WAM10 vector map (Spalding et al., 2010) was downloaded from the Ocean Data Viewer website. The WAM10 map was generated by such joint initiatives as the International Tropical Timber Organization (ITTO) and the International Society for Mangrove Ecosystems (ISME) through analyses of Landsat TM/ETM + data acquired between 1999 and 2003. Mangrove forest maps of China were respectively clipped from MFSA15 and WAM10 for comparison.

2.2.4. In-situ data for algorithm development and map accuracy assessment

We organized in-situ data from multiple sources. First, field surveys in mangrove forest protection areas in Beihai City, Guangxi ZAR, and Zhanjiang and Zhuhai cities in Guangdong Province were carried out mid-May of 2015. An additional field survey of the mangrove forest protection area in Dongzhai Harbor, Hainan Island was performed in 2012. Photos of mangrove forests and surrounding landscapes were taken by the GPS-based EX-H20G camera and uploaded to the Global Geo-Referenced Field Photo Library (www.eomf.ou.edu/photos/), a free and public portal for people to download, upload and share GPS-embedded land cover photos. These GPS photos were converted to Keyhole Markup Language (KML) format files and then loaded into Google Earth (GE). Second, in-situ data from the China Mangrove Conservation Network (CMCN, <http://www.china-mangrove.org>) were collected. The CMCN is a non-governmental cooperation platform that joins government, enterprises, and other non-government forces to support healthy development of mangrove ecosystem. The CMCN in-situ data consist of large number of GPS photos taken by volunteers over the respective locations of mangrove forest protection areas, and already overlaid with Google map (Fig. S1–S2). The integrated dataset of GPS-based field photos, CMCN in-situ data, and GE very high spatial resolution (VHSR) satellite images taken circa 2015 serves as the background reference for us to create Regions of Interests (ROIs) using $1^\circ \times 1^\circ$ grid cell for algorithm training and map accuracy assessment (Dong et al., 2013; Kou et al., 2015). Thirdly, we collected and organized available non-mangrove forest ROIs from previous studies. In Hainan Island, we had collected 1118 polygon ROIs of upland-forest, rubber plantation, water, cropland, and built-up (building) from our previous study, which were randomly created using $0.5^\circ \times 0.5^\circ$ grids with GPS field pho-

tos taken between 2011 and 2013 as well as GE VHSR images circa 2010 (Chen et al., 2016). Those ROIs located within the 25-km coastline buffer zone was selected and updated with GE VHSR images acquired circa 2015. Finally, a total of 224 and 634 polygon ROIs for mangrove forests and non-mangrove forests were obtained, respectively (Figs. 1 and S3).

We obtained training dataset from the available ROIs for algorithm development. First, out of the 224 mangrove forest ROIs, we selected six relatively large-size ROIs as training data to study the optical and SAR signatures of mangrove forests over time (Fig. 3). As mangrove forests have the unique feature of tidal inundation and differ in inundation frequency (frequently inundated, moderately inundated, and rarely (infrequently) inundated), these six mangrove forest ROIs have different inundation frequencies: two ROIs frequently inundated, one ROI moderately inundated, and three ROIs rarely inundated (see Figs. S4–S6 for details), based on the local tidal inundation information. Such a phenology-based signature analysis and algorithm development approach has been used and well documented in our previous studies of paddy rice croplands and forests (Xiao et al., 2005, 2006; Dong et al., 2016; Qin et al., 2016). Secondly, all mangrove forest pixels (9089 ha in total) in the MFSA15 dataset were used to evaluate our training ROIs during the spectral signature analysis. Only 20% of non-mangrove forest ROIs (127 ROIs) were randomly selected for algorithm development, using NOAA/NOS/NCCOS/CCMA Biogeography Branch's Design Tool for ArcGIS.

In addition to the remaining 218 mangrove forest ROIs and 80% of the non-mangrove forest ROIs (507 ROIs), we designed a $1^\circ \times 1^\circ$ systematic sampling grid and generated random polygon ROIs within individual grid cells for map accuracy assessment. This systematic sampling approach for accuracy assessment has been documented in previous publications (Qin et al., 2016). A total of 4100 random points (100 points per $1^\circ \times 1^\circ$ grid cell, 41 grid cells in total) with 15-m radius buffer zone (Area close to a pixel at 30-m spatial resolution) were generated using GEE's random function, but only 1184 points that distributed within a 25-km coastline buffer zone were kept for this study (Fig. S7). These random points were stored in KMZ file format and were identified as mangrove forests or non-mangrove forests with GE VHSR images obtained circa 2015. Out of the 1184 ROIs, only three mangrove forest points (ROIs) were obtained in this sampling design, as mangrove forest area accounts for very small fraction of the total study area. Therefore, we combined these 1184 random ROIs with the ROIs from field surveys and previous studies. Finally, we used 221 (218 plus 3) mangrove forest polygons ROIs and 1688 (507 plus 1181) non-mangrove forest polygons ROIs for map accuracy assessment. Detailed statistical information about the training data and reference data is shown in Table S1.

2.3. Phenology-based mangrove forest mapping algorithms

Three key features including: (1) evergreen trees or shrubs (greenness); (2) canopy coverage (high leaf area index); and (3) tidal inundation were proposed to identify mangrove forests as they are unique evergreen trees or shrubs at estuaries and marine shorelines where inundation by tides occurs. Time series Landsat data were used to identify these features of the mangrove forest ecosystem (Fig. 4). The criteria of $LSWI > 0$ and $EVI > 0.2$ was used to map evergreen forest in tropical America, Africa, and Asia (Xiao et al., 2009). We employed this criterion to identify the greenness of mangrove forest. Histogram analysis of annual mean NDVI and LSWI, based on training ROIs (Fig. 5a) and temporal profile analysis of NDVI/EVI/LSWI with four mangrove forest pixels from different locations (Fig. S8), indicated that a vast majority of mangrove forests have their NDVI and LSWI values greater than 0.3. Therefore, $NDVI > 0.3$ and $LSWI > 0.3$ were used as criteria to identify canopy



Fig. 3. Mangrove forest ROIs used for algorithm development: (a) frequently inundated mangrove forests in Tieshan Harbor, Guangxi ZAR, (b) moderately inundated mangrove forests in Anpu Harbor, Zhanjiang City, Guangdong Province, and (c) rarely inundated mangrove forests in Dongzhai Harbor, Hainan Province. (For interpretation of the references to color in this figure legend, the reader is referred to the web version of this article.)

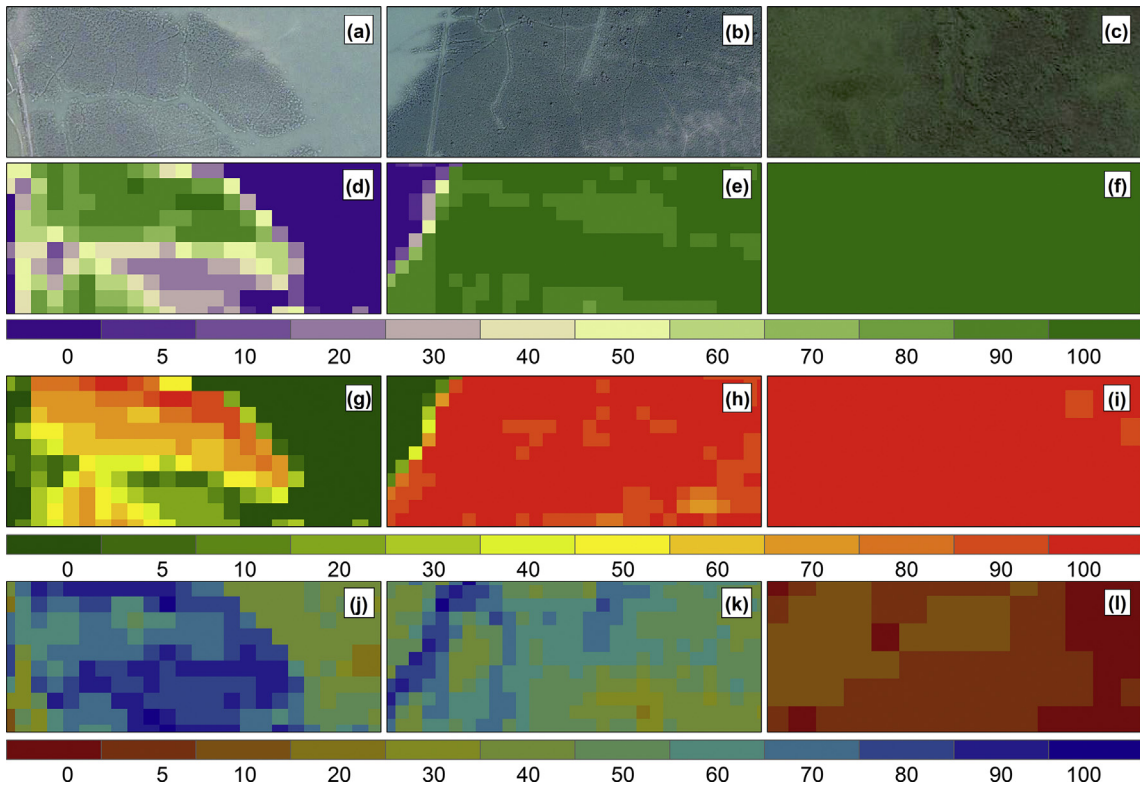


Fig. 4. Illustration of different mangrove forests in (a–c) GE VHSR images and frequency maps of (d–f) greenness, (g–i) canopy coverage, and (j–l) tidal inundation. The GE VHSR images of (a) to (c) are of frequently inundated, moderately inundated, and rarely inundated mangrove forests clipped from Fig. 3a–c, respectively. Images are matched in columns, and scale bars of greenness, canopy coverage, and tidal inundation were presented below corresponding maps. (For interpretation of the references to color in this figure legend, the reader is referred to the web version of this article.).

coverage of mangrove forest. Tidal inundation was identified by using the criteria of $LSWI \geq EVI$ or $LSWI \geq NDVI$, both of which have been used for mapping paddy rice and reed wetland (Dong et al., 2016; Zhou et al., 2016).

Because of the variation in tidal action and phenology of mangrove forests, the features of greenness, canopy coverage, and inundation from specific imagery or one image composite could be biased. Here we used frequency-based greenness, canopy coverage, and inundation from time series Landsat images to identify mangrove forest, following the method reported in mapping paddy rice in northeastern Asia (Dong et al., 2016). For greenness frequency, as an example, we first determine greenness state using Eq. (5).

$$Greenness = \begin{cases} 1 & LSWI > 0 \text{ and } EVI > 0.2 \\ 0 & \text{Other values} \end{cases} \quad (5)$$

Secondly, calculating greenness frequency using Eq. (6).

$$F_{Greenness} = \frac{\sum N_{Greenness}}{\sum N_{Total} - \sum N_{Bad}} \times 100 \quad (6)$$

where $F_{Greenness}$ is greenness frequency scaled to 0 and 100, $N_{Greenness}$ is the number of observation with $LSWI > 0$ and $EVI > 0.2$, and N_{Total} is the number of total observations, N_{Bad} is the number of bad observations (e.g. clouds, shadows, and ETM + scan-line-off strips) (Dong et al., 2016). Frequency maps of canopy coverage and tidal inundation were generated using the criteria of

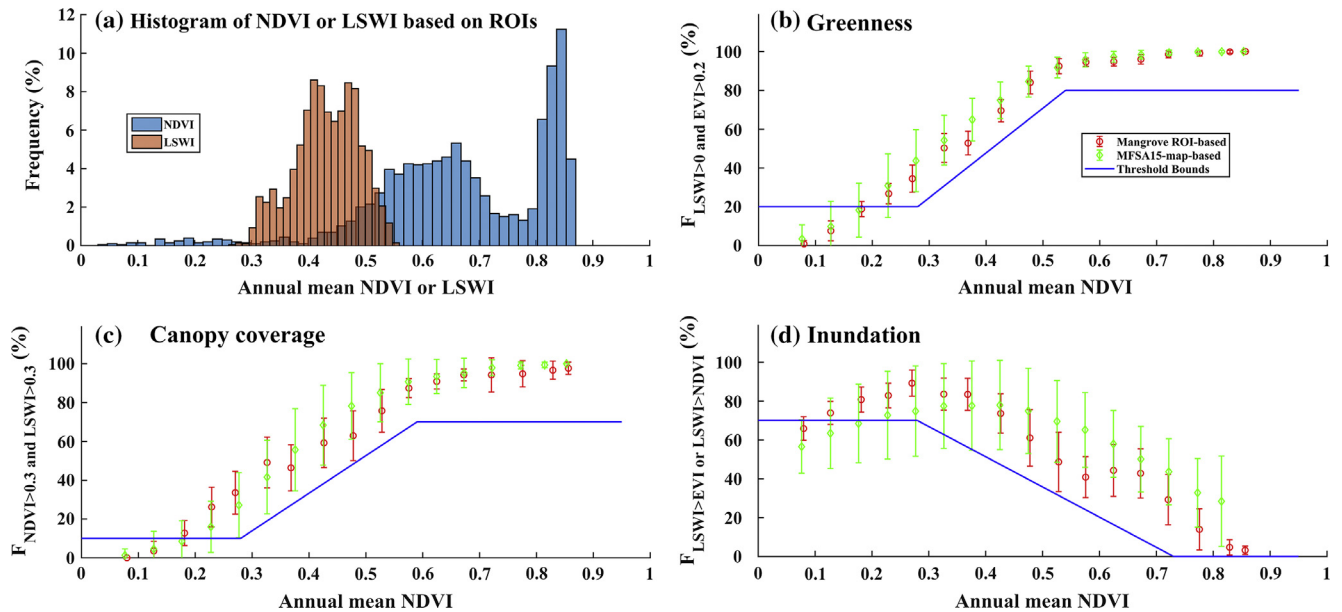


Fig. 5. The annual mean NDVI and LSWI histograms of mangrove forests based on training ROIs (a), and error bar plots of annual mean NDVI against frequency of (b) greenness, (c) canopy coverage, and (d) tidal inundation based on training ROIs and MFSA15, respectively. The error bars indicate one standard deviation, while blue lines were corresponding fitted thresholds based on $\mu - 2\sigma$ values of training ROIs. (For interpretation of the references to color in this figure legend, the reader is referred to the web version of this article.)

($NDVI > 0.3$ and $LSWI > 0.3$) and ($LSWI \geq EVI$ or $LSWI \geq NDVI$), respectively.

Determining the frequency thresholds of greenness, canopy coverage, and tidal inundation was a key step during mapping mangrove forests. Due to the spectral influence of water, frequently inundated mangrove forests (Fig. 4a) have weak signals of greenness (Fig. 4d) and canopy coverage (Fig. 4g), but strong inundation signal (Fig. 4j). Conversely, rarely inundated mangrove forests (Fig. 4c) have strong signals of greenness (Fig. 4f) and canopy coverage (Fig. 4i), but weak tidal inundation signal (Fig. 4l). The moderately inundated mangrove forests (Fig. 4b) have moderate signals of greenness, canopy coverage, and tidal inundation. Therefore, fixed frequency thresholds cannot address these situations well, and variable frequency thresholds are more appropriate.

Based on the fact that the denser the canopy, the lower the chance that water has been observed by satellites, we assume that the frequency of greenness, canopy coverage, and tidal inundation were closely related to mangrove forest canopy density, which can be represented by annual mean NDVI (Jensen et al., 1991). The frequency of greenness and canopy coverage linear increased significantly with annual mean NDVI when $NDVI < 0.6$ (Fig. 5b and c), while tidal inundation frequency decreased linearly with annual mean NDVI when $NDVI > 0.3$ (Fig. 5c). Therefore, variable frequency thresholds of greenness, canopy coverage, and tidal inundation can be determined using their linear fits against annual mean NDVI. In this study, the linear fits were built on low bound values of $\mu - 2\sigma$, where μ is annual mean NDVI and σ standard deviation (see Figs. S9–S11 for details). Based upon the mangrove forest characteristics presented in Fig. 5, the frequency upper (lower) bound thresholds for greenness, canopy coverage, and tidal inundation were set to 80% (20%), 70% (10%) and 70% (0), respectively. Therefore, based on the linear fitting results from Figs. S9–S11, mangrove forests were identified if a pixel meets (7), (8), and (9) at mean time according to its annual mean NDVI.

$$F_{greenness}(x) > \begin{cases} 20 & x < 0.25 \\ 211.47x - 33.46 & 0.25 \leq x < 0.54 \\ 80 & x \geq 0.54 \end{cases} \quad (7)$$

$$F_{Canopy}(x) > \begin{cases} 10 & x < 0.28 \\ 193.85x - 43.78 & 0.28 \leq x < 0.59 \\ 70 & x \geq 0.59 \end{cases} \quad (8)$$

$$F_{Inundation}(x) > \begin{cases} 70 & x < 0.28 \\ -155.81x + 114.01 & 0.28 \leq x < 0.73 \\ 0 & x \geq 0.73 \end{cases} \quad (9)$$

where x is annual mean NDVI.

2.4. Implementation of mangrove forest mapping algorithm in China

Implementation of the mapping algorithms (see Section 2.3) at the regional scale is a challenging task, since many factors could potentially affect classification accuracy. However, areas where mangrove forests are not likely to occur can be excluded from the spatial analysis (Long and Giri, 2011). We first created the masks of four non-mangrove land cover types: non-coastal zones, upland and steep-slope regions, built-up and barren lands, and yearlong water bodies. Second, we generated the mangrove forest map in 2015, based on spectral signatures of greenness, canopy coverage, and tidal inundation. The mangrove forest map was further refined by determining the forest's connectivity with the sea using a yearlong water body mask (Fig. 6).

2.4.1. Coastal zone regions

A 25-km coastline buffer zone was generated to delineate the potential areas of mangrove forests. This buffer extends 15 km inland and 10 km in the sea. The buffer zone boundary was modified in some regions (e.g. around Hong Kong) where the coastlines are wide, due to the presence of islands. A similar 10 km buffer zone has been used to map mangrove forests along the Kenyan coastline by Kirui et al. (2013).

2.4.2. Upland and steep-slope regions

Histograms of mangrove forest elevations and slopes, based on training ROIs and the MFSA15 map in China, indicated that a vast majority of mangrove forests were distributed in areas with an elevation between -5 m and 10 m above mean sea level (AMSL) and a

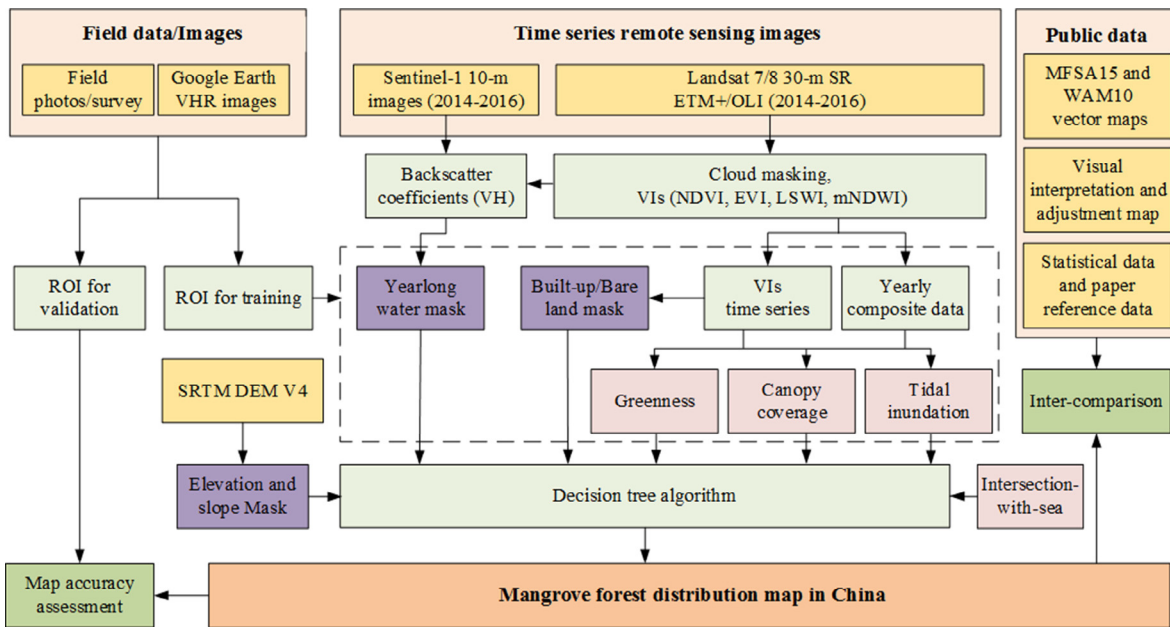


Fig. 6. Mangrove forest mapping flow chart. (For interpretation of the references to color in this figure legend, the reader is referred to the web version of this article.)

slope of less than 10° (Fig. 7). Therefore, $\text{DEM} < 10 \text{ m}$ and $\text{slope} < 10^\circ$ were used to delineate the potential locations of mangrove forests.

2.4.3. Built-up and barren lands

Built-up and barren lands have either an impervious surface or exposed soils, which usually have low LSWI values (Xiao et al., 2005). A frequency map of $\text{LSWI} < 0$ was generated using a method similar to Eq. (5) and (6). A pixel with frequency value $>50\%$ was then classified as built-up or barren land (Zha et al., 2003; Qin et al., 2015) and were masked as non-mangrove.

2.4.4. Yearlong water bodies

Along the coastline, there are a considerable amount of yearlong water bodies, such as salterns and aquaculture ponds. As illustrated in Fig. 8b&c, Sentinel-1A VH band was very sensitive to water and non-water (upland forest, built-up, and cropland) cover, and water can be readily identified using $\text{VH} < -19$. However, a few

land cover types, such as sand beaches and flat impervious surfaces like airport runways, also have $\text{HV} < -19$ (intersect area in Fig. 8c, and see Fig. S12 for illustration). These non-water land cover types can be identified by $\text{mNDWI} > 0$ used for mapping open surface water bodies (Xu, 2006). Frequency maps with $\text{VH} < -19$ and $\text{mNDWI} > 0$ were generated based on all Sentinel-1A and Landsat data, respectively (Fig. 8d&e). The boundary between water and non-water in the Sentinel-1A VH frequency map was more accurate than that of the mNDWI frequency map (Fig. 8d&e). Here we use $F_{\text{VH} < -19} > 80\%$ and $F_{\text{mNDWI} > 0} > 10\%$ to identify yearlong water bodies (Fig. 8f).

2.4.5. Refining the mangrove forest map using the intersection-with-sea criterion

Mangrove forests are usually inundated with sea water. Therefore, mangrove forest patches that do not intersect the sea at any point in the year are considered non-mangrove. A few isolated

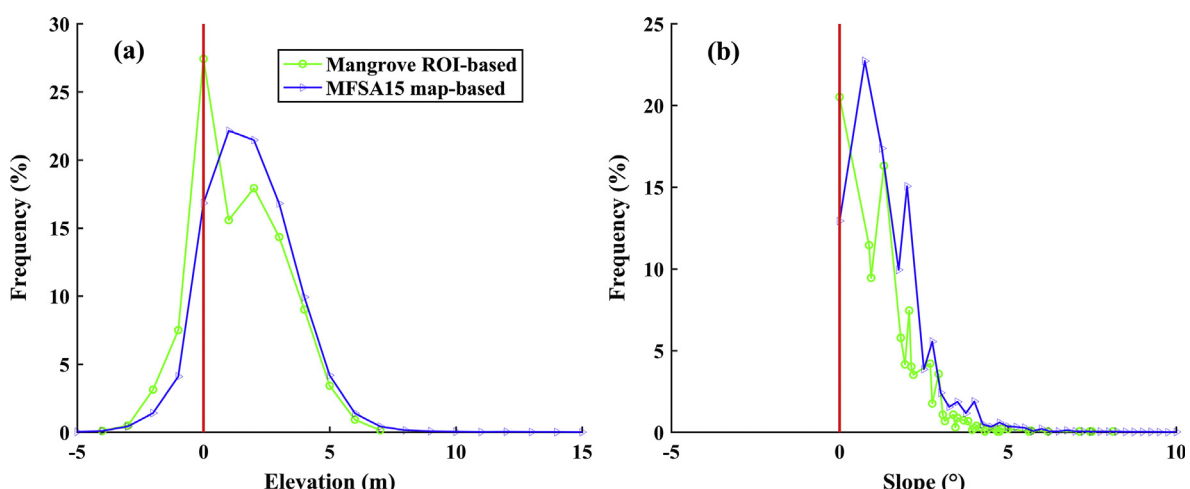


Fig. 7. Histogram of (a) elevation and (b) slope based on mangrove forest training ROIs and MFSA15, respectively. (For interpretation of the references to color in this figure legend, the reader is referred to the web version of this article.)

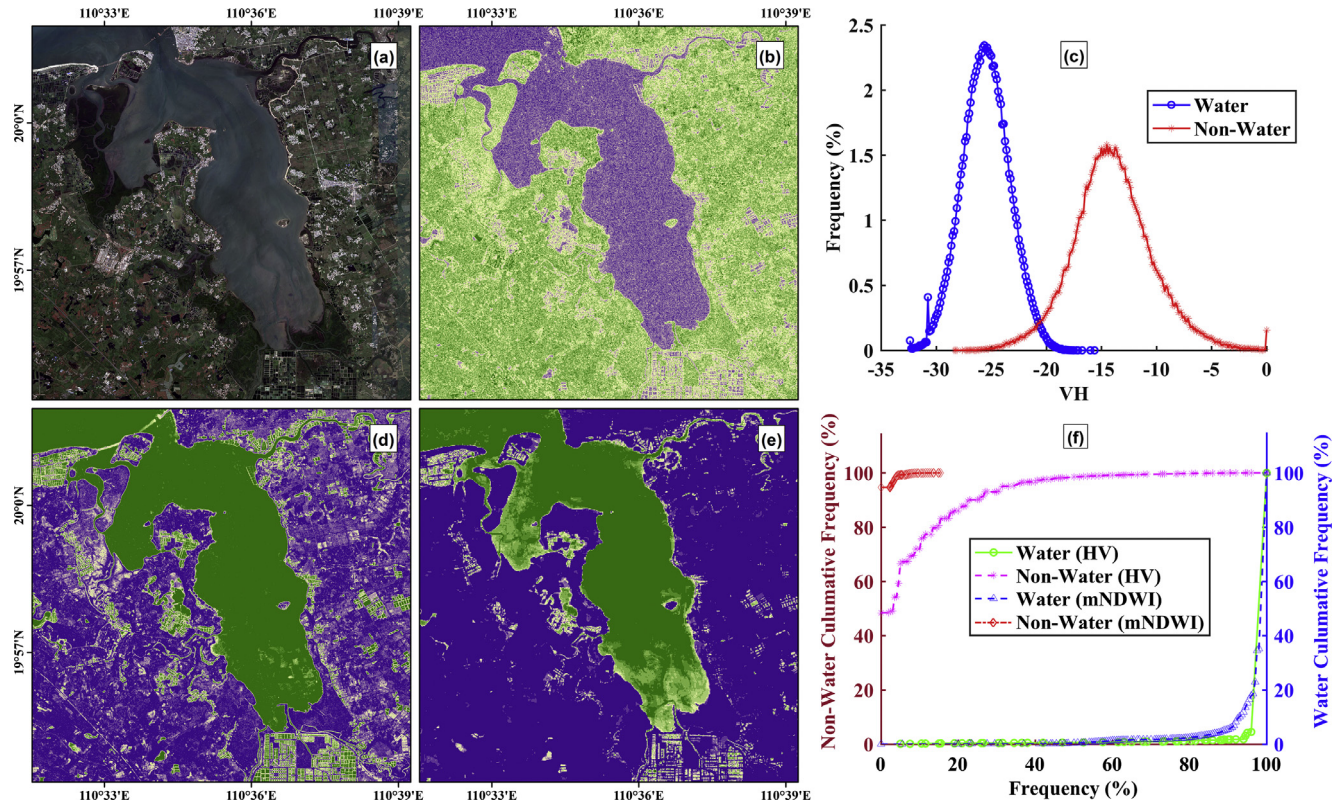


Fig. 8. Illustration of identifying yearlong water using Sentinel-1A and Landsat data: (a) GE VHSR image at Dongzhai Harbor, Haikou; (b) Sentinel-1 VH band acquired on June 25, 2015, and (c) histogram of water and non-water in image b; (d) frequency map with $VH < -19$ based on all Sentinel-1A data; (e) frequency map with $mNDWI > 0$ based on all Landsat data; (f) cumulative frequency of water and non-water ROIs based on frequency map with $VH < -19$ and $mNDWI > 0$, respectively. (For interpretation of the references to color in this figure legend, the reader is referred to the web version of this article.)

mangrove forests were removed from the map using this criterion, but their area was very small when screening the entire study area in GE. Seawater bodies were derived from yearlong water bodies by removing small inland water bodies such as aquaculture ponds. However, bays or estuaries that are separated by bridges should be kept as sea. Based on a simple testing, a threshold of 100 ha was used to remove small inland yearlong water bodies while maintaining bays and estuaries as sea. A buffer zone of 100 m was added to the seawater body layer to help determine the intersection between mangrove forest patches and the sea in GEE. Forest patches that intersected with the seawater buffer zone are kept as mangrove forests.

2.5. Accuracy assessment of the resultant mangrove forest maps

The mangrove forest map generated from the algorithm defined in this study (Digital Classified Mangrove Forest Map, MFM_{DC}) was converted to KML format in GEE. It was then loaded into GE, visually interpreted and evaluated, and adjusted (keep, remove, or add polygons) using GE VHSR images circa 2015 (Visual Interpreted and Adjusted Mangrove Forest Map, MFM_{DC+VIA}). In Guangxi ZAR, the MFM_{DC+VIA} was further confirmed by a local expert (Lianghao Pan) from the Guangxi Mangrove Research Center (GMRC), Guangxi Academy of Sciences, with ten years of field experience in the mangrove region. The KML format MFM_{DC} and MFM_{DC+VIA} were converted to a raster format at 30-m spatial resolution in ArcGIS and then loaded in ENVI for accuracy assessment using ground reference data by confusion matrix. The ground reference data consist of 221 (218 manually created and 3 computers generated) mangrove forest polygon ROIs and 1688 (507 manually created and 1181 computer generated) non-mangrove forest polygon ROIs.

The KML format of MFM_{DC} and MFM_{DC+VIA} were also converted into shapefile format in ArcGIS to calculate area using a projected coordinate system of Krasovsky_1940_Albers. Then, the percentages of spatially consistent area in different regions between the MFM_{DC} and MFM_{DC+VIA} were reported.

2.6. Inter-comparison with other available mangrove forest maps or datasets

Wall-to-wall comparisons between MFM_{DC+VIA} and the MFSA15 ([Lü et al., 2015](#)) in Guangxi ZAR and WAM10 ([Spalding et al., 2010](#)) in China were conducted, respectively. We only chose Guangxi ZAR for comparison because mangrove forests in other regions were not fully mapped in MFSA15. Mangrove forest areas at the provincial level was also compared with the following public data: 1) State Forestry Administration (SFA) ([Chen et al., 2009](#)); 2) Northeast Institute of Geography and Agroecology, Chinese Academy of Sciences (IGA-CAS) ([Jia et al., 2014](#)); 3) the First Institute of Oceanography, State Oceanic Administration (FIO-SOA), China ([Wu et al., 2013](#)); 4) MFSA15; and 5) WAM10. The MFW ([Giri et al., 2011](#)) and CGMFC-21 ([Hamilton and Casey, 2016](#)) were not compared because only about 3000 ha in Guangxi ZAR was reported in these two products. These maps were generated using images from 2002, 2010, 2010, 2015, and 2000 for SFA, IGA-CAS, FIO-SOA, MFSA15, and WAM10, respectively. Although most of these datasets were generated five or more years earlier than our map, it still has reference value given China's protection policies that have increased since the 1980s ([Chen et al., 2009](#)). In addition, most mangrove forests grow slowly; it is not likely that mangrove forests would rapidly expand within a few years.

3. Results

3.1. Accuracy assessment of the China's mangrove forest map in 2015

Both the MFM_{DC} and MFM_{DC+VIA} show high accuracy when evaluated with ground reference ROIs (**Table 2**). They shared almost same values of user's accuracy (UA), producer's accuracy (PA), overall accuracy (OA), and kappa coefficients. The UA, PA, OA, and Kappa coefficient for MFM_{DC+VIA} were 100%, 95.54%, 99.19% and 0.97, respectively.

The mangrove forest map in Guangxi ZAR had the highest accuracy; identical areas (spatially consistent mangrove forests area between MFM_{DC} and MFM_{DC+VIA}) account for 97% of the MFM_{DC} and 96% of MFM_{DC+VIA} (**Table 3**). In Guangdong, Hainan, Fujian and Hong Kong, the identical area accounts for relatively low values (82–84%) with MFM_{DC}, but high values (93–99%) with MFM_{DC+VIA}. However, the identical area can account for 94% and 97% of MFM_{DC} in Guangdong and Hainan Province, respectively, if only those regions with dense mangrove forest cover are considered. The consistent areas between MFM_{DC} and MFM_{DC+VIA} are low in Taiwan and Macao, and especially low in Zhejiang (**Table 3**). The identical area in China are 86% and 96%, when compared with the MFM_{DC} and MFM_{DC+VIA}, respectively (**Table 3**).

3.2. Spatial and area distribution of mangrove forests in China in 2015

Mangrove forests in China are mostly distributed along the coastlines of Guangxi ZAR, Guangdong Province, and the northern part of Hainan Province. Mangrove forest cover decreased significantly from the coastline of Hong Kong north to Zhejiang Province (**Fig. 9a**). In Taiwan, mangrove forests are mainly distributed along the western and northwest coastline. The total area of mangrove forests from MFM_{DC+VIA} is 20,303 ha, with 6849 ha, 8136 ha, and 3667 ha in Guangxi ZAR, Guangdong, and Hainan Provinces, respectively (**Table 4**). These three regions account for about 92% of the total mangrove forest cover in China. Mangrove forest cover in Fujian Province, Taiwan, and Hong Kong range from 410 ha to 675 ha. About 8 ha and 13 ha of mangrove forests are found in Zhejiang Province and Macao, respectively.

3.3. Inter-comparison of mangrove forest maps among multi-source datasets

The identical area between MFM_{DC+VIA} and MFSA15 in Guangxi ZAR is 3992 ha, accounting for 80% of MFSA15 and 58% of MFM_{DC+VIA}, respectively (**Fig. 10**). A considerable amount of mangrove forests around the bay of Qinzhou City (black boxes of I and II) occurs in MFM_{DC+VIA} but not in MFSA15. These regions do contain a great deal of mangrove forests (**Fig. 10b&c**). The 1017 ha of mangrove forests that are only mapped in MFSA15 is due to the difference in patch boundaries and misclassification (**Fig. 10d**).

There are large differences between MFM_{DC+VIA} and WAM10 (**Fig. 11**). The spatially consistent area between these two maps

is 9546 ha, accounting for only 47% of MFM_{DC+VIA} and 48% of WAM10, respectively. The MFM_{DC+VIA} has more mangrove forests in Guangxi ZAR (e.g. **Fig. 11c**) and Guangdong Province (e.g. **Fig. 11b**) than WAM10, but fewer mangrove forests in Fujian and Zhejiang Province (e.g. **Fig. 11a** in purple box). For some regions, such as Hong Kong, mangrove forests of WAM10 have several pixels of geometry offsets (**Fig. 11b**). The WAM10 also detected many more mangrove forests at Tongmingwan, Zhanjiang City, Guangdong Province, where large patches of mangrove forests might have existed before this study (**Fig. 11d**).

The total area of mangrove forests in China from MFM_{DC+VIA} (20,303 ha) is very close to the area from WAM10 (19,788 ha) and IGA-CAS (20,778 ha) and lower than the area calculated from the SFA (22,025 ha) and FIO-SOA (24,578 ha) (**Table 4**). At the provincial level, we detected more mangrove forests in Guangxi ZAR than most studies except SFA (8375 ha). In Guangdong Province, we mapped 8136 ha of mangrove forests, obviously lower than the area from FIO-SOA (12,131 ha) and about 1000 ha lower than SFA and IGA-CAS. The area of mangrove forests in Hainan Province differs slightly among these studies, except FIO-SOA (4891 ha). WAM10 has detected significantly higher values of mangrove forests than the other studies in Fujian and Zhejiang Province. We detected 544 ha of mangrove forests in Hong Kong, very close to the agricultural statistics data (510 ha) reported by the Agriculture, Fisheries and Conservation Department of Hong Kong.

4. Discussion

4.1. Data and algorithms for mapping mangrove forests

This study developed a new algorithm to identify mangrove forests based on its unique features and applied this algorithm using time series data from Landsat and Sentinel-1A, as well as DEM, to map China's mangrove forests in 2015. The algorithms and data used in this study are quite different from several previous studies (De Santiago et al., 2013; Giri et al., 2015; Jhonnerie et al., 2015).

First, the integration of Landsat optical and Sentinel-1A SAR data captures complementary information on the spectral and structural characteristics of mangrove forests. We also use both Sentinel-1A and Landsat data to generate a yearlong water mask, which is valuable for the identification of mangrove forests via their inundation by the sea. Previous studies have used a supervised classification approach (Giri et al., 2011), NIR band (Long and Skewes, 1996), and brightness (Vo et al., 2013) to map water bodies before mapping mangrove forests. Although NDWI or modified NDWI (mNDWI) derived from Landsat data were good indicators of open surface water bodies (Mcfeeters, 1996; Xu, 2006; Rokni et al., 2014), the inclusion of Sentinel-1A data was still useful since it has a fine spatial resolution of 10-m and is unaffected by cloud cover. We found Sentinel-1A VH band differentiates well between water and non-water, as the frequency map with VH < -19 has a more distinct boundary between water and non-water than does the frequency map with mNDWI > 0 (**Fig. 8d&e**).

Table 2
Accuracy assessment of MFM_{DC} and MFM_{DC+VIA} in China using ground reference data.

Class	Ground reference pixels		Total map pixels	User's accuracy
	Mangrove	Non-mangrove		
Map pixels	Mangrove	7204/7155	0/1	7204/7156
	Non-mangrove	359/334	32,868/33,819	34,227/34,163
Total ground truth pixels		7563/7489	32,868/33,820	41,431/41,309
Producer's accuracy		95.25%/95.54%	100%/100%	

Overall accuracy is 99.13%/99.19% and kappa coefficient is 0.97/0.97, respectively. The first values before backslash in each cell were for MFM_{DC}, and the second were for MFM_{DC+VIA}. Non-mangrove includes upland-forest, cropland, water, and built-up lands.

Table 3Comparison between the MFM_{DC} and MFM_{DC+VIA} in 2015.

	Mangrove forest area (ha)			Percentage (%)	
	MFM _{DC}	MFM _{DC+VIA}	Identical	Identical/MFM _{DC}	Identical/MFM _{DC+VIA}
Guangxi ZAR ^a	6775	6849	6572	97	96
Guangdong/DMFR	9565/6927	8136/6728	7919/6528	83/94	97/97
Hainan/DMFR	4136/3467	3667/3562	3417/3346	83/97	93/94
Fujian	807	675	662	82	98
Hong Kong	645	544	539	84	99
Taiwan	707	410	387	55	94
Zhejiang	13	8	2	15	25
Macao ^b	6	13	5	83	38
Total	22,654	20,303	19,503	86	96

MFM_{DC}: Mangrove forest map direct from digital classification; **MFM_{DC+VIA}**: MFM_{DC} after visual interpretation and adjustment using GE VHSR images; **Identical**: Identical mangrove forest area between MFM_{DC} and MFM_{DC+VIA}; **DMFR**: Dense mangrove forest region, corresponding spatial extents were shown in Fig. 9(I and III);

^a MFM_{DC+VIA} here was additionally confirmed by a local expert with ten years of field experience.

^b Classified accuracy would be close to 100% but degraded significantly due to influence of a conical building, see Fig. S13 for detail.

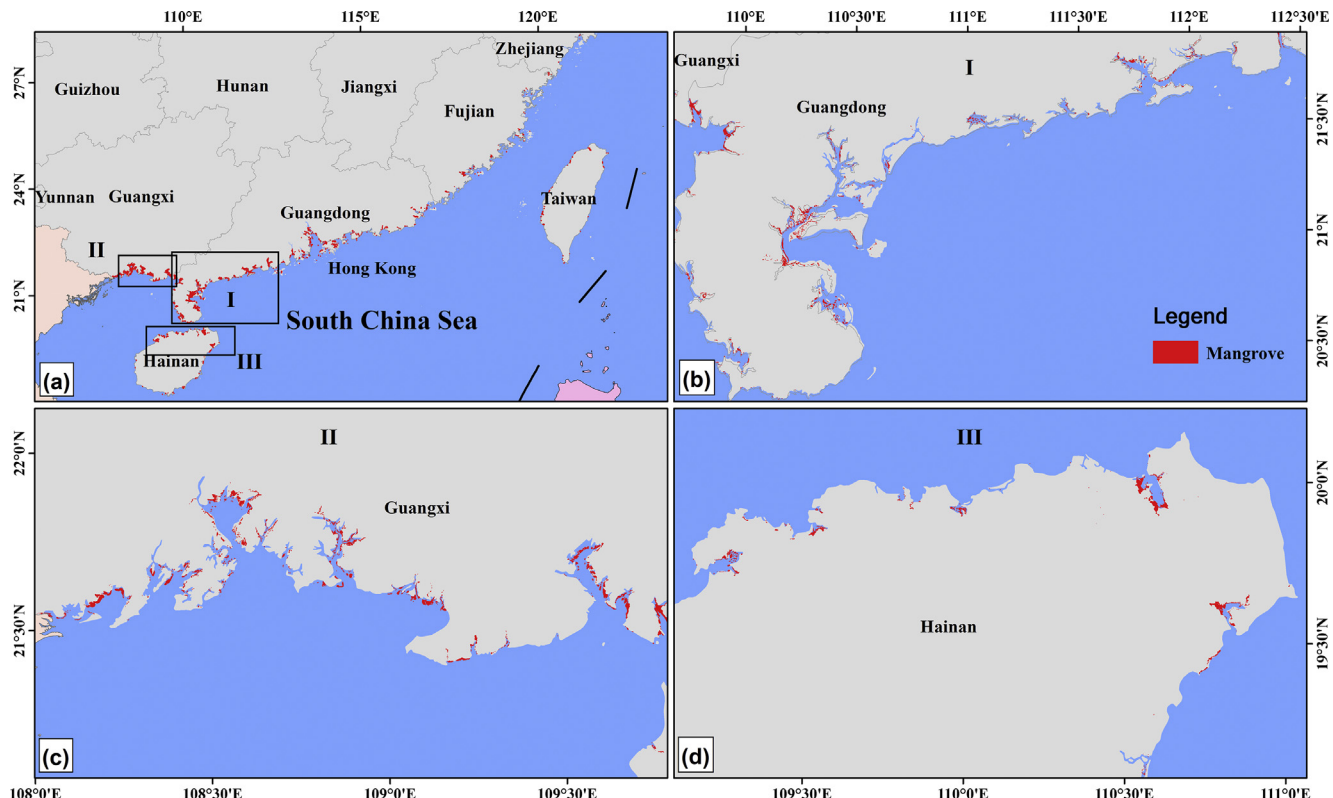


Fig. 9. Spatial distribution of (a) China's mangrove forests in 2015 and (b) zoom views of extent I in Guangdong Province, (c) extent II in Guangxi ZAR and (d) extent III in Hainan Province where dense mangrove forests occurs. (For interpretation of the references to color in this figure legend, the reader is referred to the web version of this article.)

The mNDWI, however, is useful in eliminating misclassified water pixels such as sand beaches and flat impervious surfaces from the Sentinel-1A based water map.

Secondly, classification of mangrove forests based on time series Landsat imagery greatly reduced misclassification typically caused by the effects of tidal inundation on vegetation indices (Cohen and Lara, 2003; Wu et al., 2013). In order to reduce this tidal inundation effect, some studies used satellite data obtained during low tide to map coastal vegetation like mangrove forests (Nayak and Bahuguna, 2001). Most previous studies used images of single date or multi-date mosaics for mangrove forest classification (Table 1), while we used frequency-based criteria from three years of time series Landsat and Sentinel-1 data. The resultant mangrove forest maps for 2015 have high accuracy (UA/PA/

OA > 95%) and are more robust than those derived from analyses of single/mosaic images (e.g. MFSA15), as the advantages of land cover classification based on time series image data have been illustrated by several studies (Hermosilla et al., 2015; Reiche et al., 2015; Dong et al., 2016; Zhou et al., 2016).

Thirdly, most prior studies employed supervised (e.g., MLC) and unsupervised (e.g., ISODATA) classification algorithms to map mangrove forests or to quantify their changes (Table 1). The resultant maps are often affected by the training datasets and selected images used in the analysis, which makes it hard to compare maps from different years or data producers. In this study, we used three key features: greenness, canopy coverage, and tidal inundation to map mangrove forests. Time series Landsat ETM+/OLI data accurately captures these features and enables us to distinguish man-

Table 4

Area comparison of mangrove forests in China from different map data sources.

	Mangrove forest area (ha)					
	This study (2015)	SFA (2002)	IGA/CAS (2010)	FIO/SOA (2010)	WAM10 (2000)	MFSA15 (2015)
Guangxi	6849	8375	5813	6596	4529	5009
Guangdong	8136	9084	9289	12,131	7276	4080*
Hainan	3667	3930	3576	4891	3919	—
Fujian	675	615	1023	941	2186	—
Zhejiang	8	21	293	20	1188	—
Taiwan	410	—	382	—	242	—
Hong Kong	544	—	389	—	448	—
Macao	13	—	11	—	—	—
Total	20,303	22,025	20,778	24,578	19,788	9089

SFA: State Forestry Administration, from Chen et al. (2009); **IGA/CAS:** Northeast Institute of Geography and Agroecology, Chinese Academy of Sciences, from Jia et al. (2014); **FIO/SOA:** First Institute of Oceanography, State Oceanic Administration, from Wu et al. (2013); **WAM10:** World Atlas of Mangroves (2010) from Spalding et al. (2010); **MFSA15:** Mangrove Forest map in South Asia in 2015, from Lü et al. (2015).

* Mangrove forest mapping in Guangdong Province was incomplete in MFSA15.

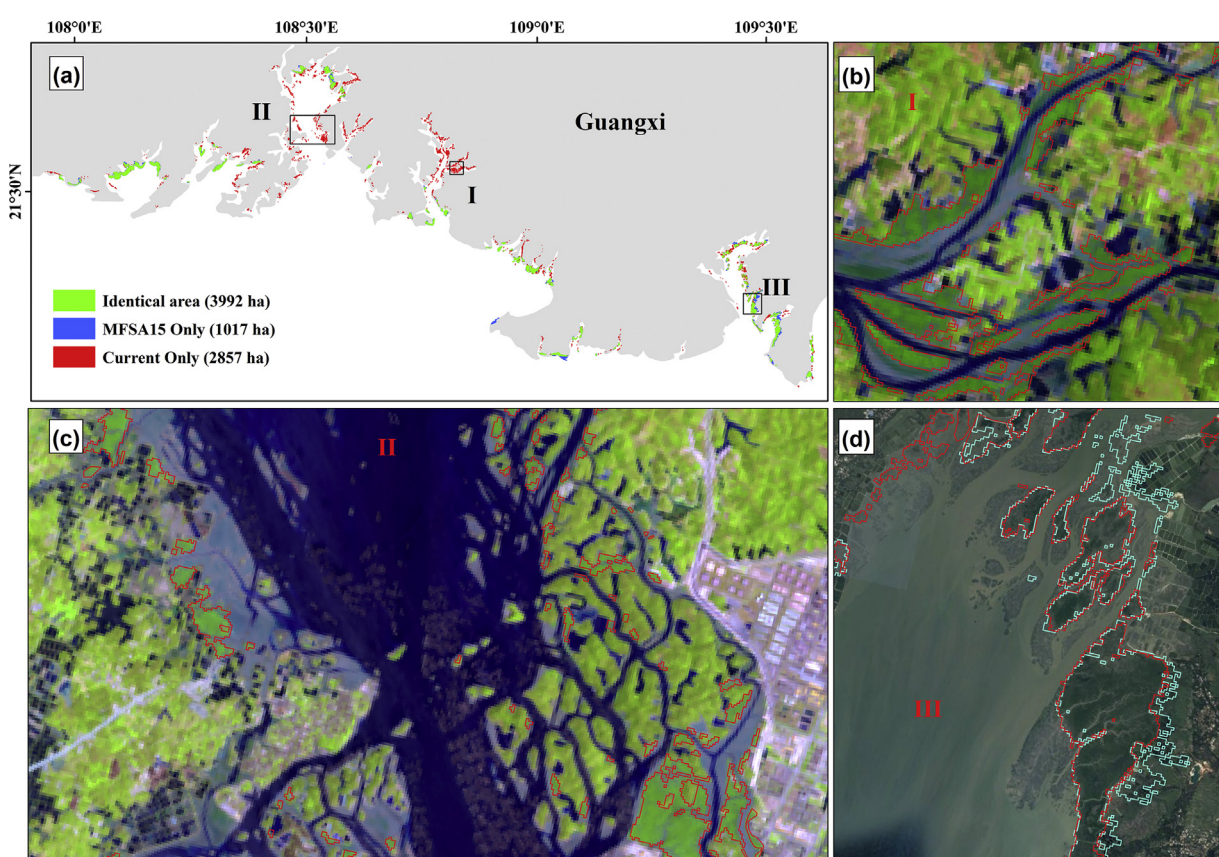


Fig. 10. Spatial comparison between MFM_{DC+VI} and MFSA15 in Guangxi ZAR: (a) overlay comparison with identical areas in green and inconsistent areas in red and blue, zoom views of extent I (b) and extent II (c) where mangrove was not mapped in MFSA15, and (d) zoom view of extent III where inconsistency was existed between MFM_{DC+VI} (in red) and MFSA15. The background of (b) and (c) are Landsat OLI images acquired on April 14, 2015 (P124/R45) shown in false color composite (R/G/B = Band 6/5/4), while the background in (d) is a GE VHSR image acquired on October 8, 2015. (For interpretation of the references to color in this figure legend, the reader is referred to the web version of this article.)

grove forests from other land cover types. This phenology-based algorithm requires a relatively small number of training datasets (we used 6 mangrove ROIs here) to study how mangrove forests change over time. It can be applied as a more general classification algorithm that can be readily extended to large regions with the GEE platform. We also found that the annual mean NDVI is a key variable in determining the frequency thresholds of greenness, canopy coverage, and tidal inundation, which allows us to generate mangrove forest maps in China using one algorithm and dynamic threshold values.

Fourthly, removing forest patches not intersecting with the sea was a simple and straightforward method to refine mangrove for-

est maps. Previous study used a similar intersection criterion with water and noncontiguous water to refine mangrove forest maps during post-classification in GIS software (Long and Skewes, 1996). Here, we integrated these steps with GEE and generated a map directly. Fig. 12 illustrates the implementation of this intersection-with-sea criterion. Many discrete patches in red were previously misclassified as mangrove forests (Fig. 12A), and most have been removed as they are not inundated by the sea (Fig. 12d). In addition, buffer zone, elevation, and slope were employed in the analysis to generate mangrove forest maps. The thresholds for these criteria was similar or the same as in previous studies. For example, Almahasheer et al. (2016) used a 1-km buffer

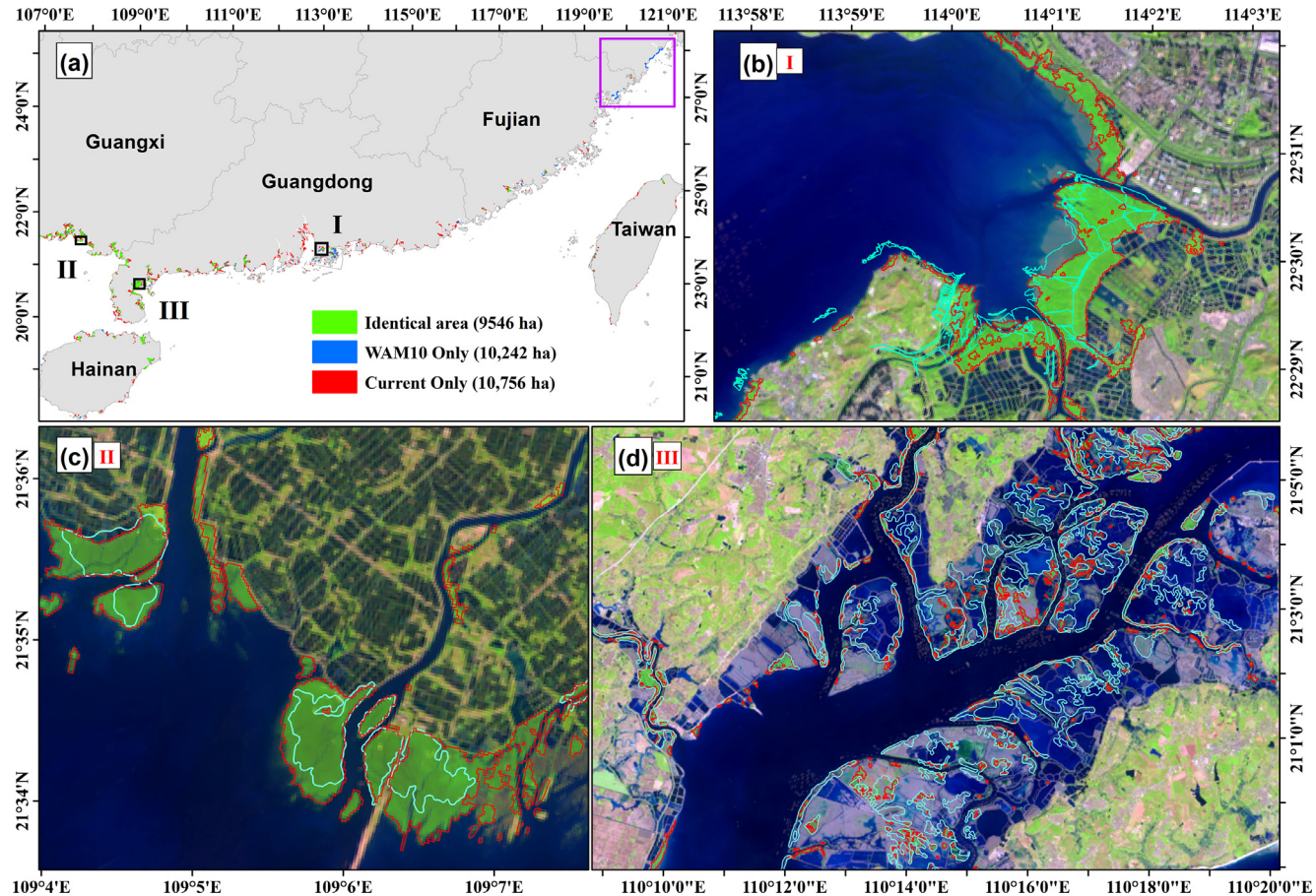


Fig. 11. Spatial comparison between MFM_{DC+VI} and WAM10: (a) overlay comparison with identical areas in green and inconsistent areas in red and blue; (b) zoom view of Mai Po Marshes Nature Reserve in Hong Kong and borders of Shenzhen Special Economic Zone of Guangdong Province (extent I) where mangrove forests in Shenzhen were not mapped and geometry offsets existed in the WAM10 map; (c) zoom view of extent II in Beihai City, Guangxi ZAR where some mangrove forests were not mapped in WAM10; and (d) zoom view of extent III in Tongminwan, Zhanjiang City, Guangdong Province where the WAM10 mapped many more mangrove forests. The purple rectangle in (a) indicates the WAM10 map here almost classification error because natural limits of mangrove forests in China is about 27°N. The background of (b), (c) and (d) are Landsat OLI images acquired on January 19, 2015 (P122/R44), October 23, 2015 (P125/R45) and January 17, 2015 (P124/R45) shown in false color composite (R/G/B = Band 6/5/4), respectively. (For interpretation of the references to color in this figure legend, the reader is referred to the web version of this article.)

from coastline to mask out non-mangrove areas. Here, we used a wide buffer zone of 25-km to account for the diversity (e.g. many small islands and longer inner estuaries) of the lengthy coastline in China. The 10-m AMSL from this study was consistent with many previous studies (Long and Skewes, 1996; Kirui et al., 2013; Darmawan et al., 2016). We masked by slope because mangrove forests occur in wetlands, which have relatively flat topography.

4.2. Potential sources of errors in the resultant mangrove forest map in China

4.2.1. Evergreen vegetation that is close to yearlong water bodies

Some evergreen vegetation that is in close proximity to yearlong water bodies such as aquaculture ponds, estuaries, and the sea may be mapped as mangrove forests since these pixels were a mixture of evergreen vegetation and water (Fig. 13a). It's difficult to remove them using the intersection-with-sea criterion because they are very close to yearlong water bodies. The proportion of these misclassified pixels would be significant when mangrove forests are sparsely distributed along a coastline. For example, the identical area accounts for 55% of the MFM_{DC} in Taiwan mainly because only 410 ha of mangrove forests are distributed along its longer coastline (Table 3, Fig. 9). Sparse mangrove forests along

the coastline of south Hainan Island, Pearl River Delta—one of the most intensive disturbance estuaries – and Fujian Province also degraded the proportion of identical area to MFM_{DC} and MFM_{DC+VIA} to 82–83%. However, this type of misclassification decreased significantly in regions with relative dense distributions of mangrove forests. The identical area accounts for 97%, 94% and 97% of MFM_{DC} in Guangxi ZAR, and dense mangrove forest regions of Guangdong and Hainan Province, respectively (Table 3).

4.2.2. Young and newly planted mangrove forests

China's government has made great efforts to restore mangrove forests since the 1990s: about 1531 ha of mangrove forests have been successfully restored up to 2002, and the restoration area has continued to increase in the recent decade (Chen et al., 2009). However, most of these planted mangrove forests have a sparse canopy because they grow slowly (Fig. 13c &d), and were not identified as mangrove forests by our algorithm. This was the main reason for the 15% consistent area between MFM_{DC} and MFM_{DC+VIA} in Zhejiang Province where natural mangrove forests are rare (Spalding et al., 2010) and almost all mangrove forests were planted in recent years. It's also difficult to identify the young and newly planted mangrove forests in GE VHSR images without a wealth of field experience. Therefore, the total area of 20,303 ha

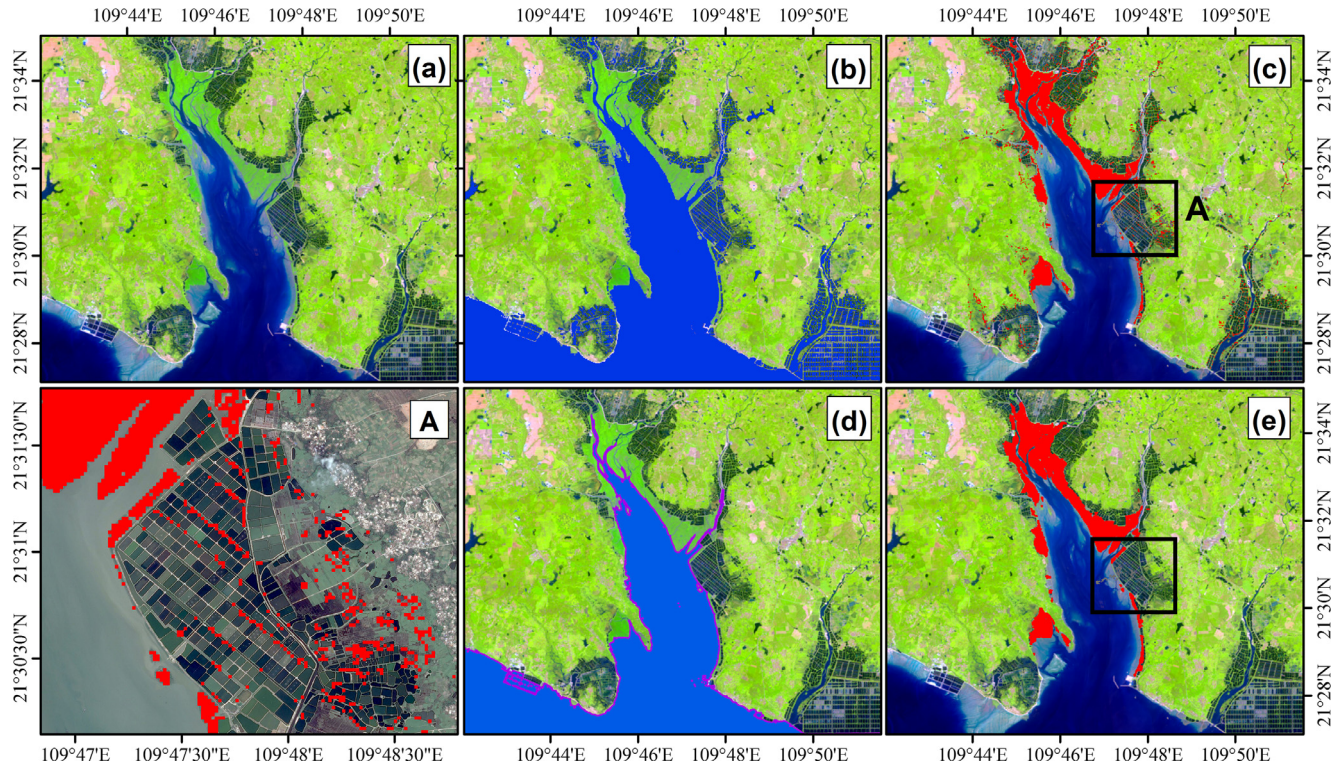


Fig. 12. Illustration of improved map accuracy using the intersection-with-sea criterion: (a) Landsat 8 OLI image acquired on September 14, 2015 shown in false color composite ($R/G/B = \text{Band } 6/5/4$) with mangrove forests shown in dark green; the OLI image overlapped with (b) yearlong water raster layer, (c) MFM_{DC} raster layer, (d) yearlong water vector layer after removing small water patches and (e) improved mangrove forest map after removing misclassified pixels that were not connected with sea. A is a zoom view of misclassified mangrove forests in a region where there was no connection to the sea. (For interpretation of the references to color in this figure legend, the reader is referred to the web version of this article.)



Fig. 13. Illustration of typical uncertainties in our algorithm: (a) typical evergreen vegetation located very close to yearlong water bodies and subsequently misclassified as mangrove forests (In red polygons); (b) isolated mangrove forests (111.00935E, 19.67804N) due to human disturbance in Tonggulin, Wenchang City, Hainan Province; (c) planted mangrove forests (108.49370E, 21.84820N) from GE VHSR at Tuanhe Island, Qinzhou City, Guangxi ZAR; and (d) field photo taken at Tuanhe Island. (For interpretation of the references to color in this figure legend, the reader is referred to the web version of this article.)

mangrove forests may slightly underestimate the total area with mangrove trees in China.

4.2.3. Isolated mangrove forests

Isolated mangrove forests (Fig. 13b) and those that have narrow connections to seawater, may not fit the intersection-with-sea criterion. Although such mangrove forest areas are likely to be very small in southern China, the applicability of this algorithm to other regions in the world needs to be explored.

4.2.4. Other land cover types

Some buildings and moving objects such as boats and ships would affect the signals of both optical and SAR data, which create some errors during water body identification and therefore affect mangrove forest mapping. For example, we detected a strong cross scatter in Sentinel-1A data in Macao (Fig. S13c). This cross scatter was caused by a building with a conical roof and separated the yearlong water bodies mapped by Sentinel-1A VH band into small pieces. About 8 ha of patchy mangrove forests was excluded by the intersection-with-sea criterion and therefore lead to very low consistency between MFM_{DC} and MFM_{DC+VIA} (Table 3).

4.2.5. Directional reflectance effects

A number of studies have suggested the need for minimizing near-nadir Landsat bidirectional reflectance (BRDF) effects to provide more consistent reflectance data over space and time (Flood, 2013; Nagol et al., 2015; Roy et al., 2016). The $\pm 7.5^\circ$ variation in view zenith angle can results in as much as 20% along scan variation in reflectance at the lower latitude sites, and the impact of variation in solar zenith angle is significant in tropics due to the relative proximity of Landsat scans to the principle plane (Nagol et al., 2015). Accounting or correction of BRDF effects (e.g. incorporating corrections for effects of sun-target-sensor geometry) would improve the mapping accuracy of mangrove forests, but not considered in this study because of ready-to-use data or algorithm are not available in GEE right now.

4.2.6. The value of visual interpretation and area adjustment

Accurately mapping mangrove forests at a regional scale is a challenging task, especially in those regions that have varying densities of mangrove forests along lengthy coastlines. As mangrove forests cover a very small percentage of Earth's surface, visual interpretation has been widely used to map mangrove forests or to improve map accuracy (Long and Skewes, 1996; Giri et al., 2011; Rodrigues and Souza-Filho, 2011; De Santiago et al., 2013; Vo et al., 2013; Wu et al., 2013; Carney et al., 2014; Jia et al., 2014). Our algorithm can reduce the number of misclassified pixels in those regions that have sparse mangrove forest cover by using stricter thresholds (e.g. higher frequency thresholds), but mangrove forests that are frequently or rarely inundated, or have sparse canopy, could also be eliminated (e.g. a lot of hollow in mangrove patches) (Fig. 4a&c). A compromising strategy was to use slightly looser thresholds (e.g. linear fits with $\mu - 2\sigma$ values) to identify most mangrove forests, then adjust it with the aid of GE VHSR images and raster MFM_{DC} that without use of the intersection-with-sea criterion. In the case with no available VHSR imagery, false color composite (R/G/B = Band 5/4/3) of Landsat cloud-free images was another good option for visual interpretation, because healthy mangrove forests always appear very dark green (Spalding et al., 2010). The visual adjustment usually includes: (1) deleting obvious misclassification patches (or polygons) and (2) adding mangrove forest polygons in areas where the intersection-with-sea criterion was not met. Unlike direct visual interpretation, the adjustment of vector MFM_{DC} was conducted very quickly by simply deleting/adding polygons, while polygon boundaries from MFM_{DC} rarely needed modification. In

addition, the algorithm performs well in regions with a relatively dense distribution of mangrove forests (Table 3).

4.3. Comparison with other available maps of mangrove forests

The differences between MFM_{DC+VIA} and other vector maps and data can be explained by several factors. First, other remote sensing-based studies used moderate spatial optical images (e.g. Landsat TM/ETM+, HJ-1A/B) from a single date or a mosaic to generate mangrove forest maps of China. Classification with limited observations may be affected by tidal variability and other factors. Second, the quality of data sources and classification methods have significant impacts on the results. For example, mangrove forest area map results in Guangdong Province varied largely from multispectral imagery of CBERS-02B and HJ-1 A/B, and the visual interpretation method (Wu et al., 2011, 2013). The WAM10 map, derived from a combination of visual interpretation and unsupervised classification, shows large classification errors in Fujian and Zhejiang Province where natural mangrove forests in China is limited to about 27°N (Spalding et al., 2010). Thirdly, some maps like WAM10 and WFM were generated more than ten years ago, and deforestation may create inconsistency between these maps (Fig. 11d). The differences between MFM_{DC+VIA} and WAM10 were mainly caused by (1) classification error, (2) change in land cover type, and (3) geometric offset of some mangrove forests in WAM10 (Fig. 11).

5. Conclusion

The mangrove forest ecosystem and the organisms they support are of significant ecological and socio-economic value. Effective classification algorithms are highly desirable for monitoring mangrove forests across local, regional, and global scales. The increasing amount of publicly available time series optical and SAR data, and cloud platforms such as GEE, have provided an opportunity to map mangrove forests using time series data approaches. By observing spatial-temporal changes in mangrove forest ecosystems, we have established a new algorithm using the frequency of greenness, canopy coverage, and tidal inundation from time series Landsat ETM+/OLI data, Sentinel-1A, and DEM data. Application of this algorithm in China yields a reliable mangrove forest map of China in 2015 with high accuracy when validated with ground-reference data (UA/PA/OA > 95%). The resultant map is also spatially consistent with mangrove forest maps that are public and visually adjusted. The total area of China's mangrove forests in 2015 was 20,303 ha, about 92% of which were distributed in Guangxi ZAR, Guangdong Province, and Hainan Province. This study has demonstrated the potential of this algorithm for mangrove forest mapping in China. It is feasible to implement the algorithm at continental and global scales on the GEE platform, after the thresholds and the intersection-with-sea criterion are carefully investigated.

Acknowledgements

This research was funded in part by research grants from the National Natural Science Foundation of China (41571408), the Central Public-interest Scientific Institution Basal Research Fund for Chinese Academy of Tropical Agricultural Sciences (Nos. 1630022015012, 1630022017016), and the US NASA Land Use and Land Cover Change program (NNX11AJ35G, NNX14AD78G). We thank the U.S Geological Survey (USGS) EROS Data Center, European Space Agency (ESA), Global Change Research Data publishing & Repository, Ocean Data Viewer for their data sources, and Google for their GEE platform. We thank Sarah Xiao at Yale

University for English editing of the manuscript. We thank four reviewers for their comments and suggestions on previous versions of the text. Their help substantially improved the manuscript.

Appendix A. Supplementary materials

Supplementary data associated with this article can be found, in the online version, at <http://dx.doi.org/10.1016/j.isprsjprs.2017.07.011>. These data include Google maps of the most important areas described in this article.

References

- Abdul Aziz, A., Phinn, S., Dargusch, P., 2015. Investigating the decline of ecosystem services in a production mangrove forest using Landsat and object-based image analysis. *Estuar. Coast. Shelf Sci.* 164, 353–366.
- Almahasheer, H., Aljowair, A., Duarte, C.M., Irigoien, X., 2016. Decadal stability of Red Sea mangroves. *Estuar. Coast. Shelf Sci.* 169, 164–172.
- Carney, J., Gillespie, T.W., Rosomoff, R., 2014. Assessing forest change in a priority West African mangrove ecosystem: 1986–2010. *Geoforum* 53, 126–135.
- Chen, B., Li, X., Xiao, X., Zhao, B., Dong, J., Kou, W., Qin, Y., Yang, C., Wu, Z., Sun, R., Lan, G., Xie, G., 2016. Mapping tropical forests and deciduous rubber plantations in Hainan Island, China by integrating PALSAR 25-m and multi-temporal Landsat images. *Int. J. Appl. Earth Obs.* 50, 117–130.
- Chen, L., Wang, W., Zhang, Y., Lin, G., 2009. Recent progresses in mangrove conservation, restoration and research in China. *J. Plant Ecol.* 2, 45–54.
- Cohen, M.C.L., Lara, R.J., 2003. Temporal changes of mangrove vegetation boundaries in Amazonia: Application of GIS and remote sensing techniques. *Wetl. Ecol. Manage.* 11, 223–231.
- Conchedda, G., Durieux, L., Mayaux, P., 2008. An object-based method for mapping and change analysis in mangrove ecosystems. *ISPRS J. Photogramm.* 63, 578–589.
- Darmawan, S., Takeuchi, W., Nakazono, E., Parwati, E., Dien, V.T., Oo, K.S., Wikantika, K., Sari, D.K., 2016. Characterization and spatial distribution of mangrove forest types based on ALOS-PALSAR mosaic 25m-resolution in Southeast Asia. In: 8th IGRSM International Conference and Exhibition on Remote Sensing & GIS.
- De Santiago, F.F., Kovacs, J.M., Lafrance, P., 2013. An object-oriented classification method for mapping mangroves in Guinea, West Africa, using multipolarized ALOS PALSAR L-band data. *Int. J. Remote Sens.* 34, 563–586.
- Donato, D.C., Kauffman, J.B., Murdiyarso, D., Kurnianto, S., Stidham, M., Kanninen, M., 2011. Mangroves among the most carbon-rich forests in the tropics. *Nat. Geosci.* 4, 293–297.
- Dong, J., Xiao, X., Chen, B., Torbick, N., Jin, C., Zhang, G., Biradar, C., 2013. Mapping deciduous rubber plantations through integration of PALSAR and multi-temporal Landsat imagery. *Remote Sens. Environ.* 134, 392–402.
- Dong, J., Xiao, X., Menarguez, M.A., Zhang, G., Qin, Y., Thau, D., Biradar, C., Moore III, B., 2016. Mapping paddy rice planting area in northeastern Asia with Landsat 8 images, phenology-based algorithm and Google Earth Engine. *Remote Sens. Environ.* 185, 142–154.
- FAO, 2007. The world's mangroves 1980–2005. FAO forestry paper, 153, Rome: Food and Agriculture Organization of the United Nations.
- Farr, T.G., Rosen, P.A., Caro, E., Crippen, R., Duren, R., Hensley, S., Kobrick, M., Paller, M., Rodriguez, E., Roth, L., Seal, D., Shaffer, S., Shimada, J., Umland, J., Werner, M., Oskin, M., Burbank, D., Alsdorf, D., 2007. The shuttle radar topography mission. *Rev. Geophys.* 45.
- Flood, N., 2013. Testing the local applicability of MODIS BRDF parameters for correcting Landsat TM imagery. *Remote Sens Lett.* 4, 793–802.
- Gao, B., 1996. NDWI—A normalized difference water index for remote sensing of vegetation liquid water from space. *Remote Sens. Environ.* 58 (1996), 257–266.
- Giri, C., Long, J., Abbas, S., Murali, R.M., Qamer, F.M., Pengra, B., Thau, D., 2015. Distribution and dynamics of mangrove forests of South Asia. *J. Environ. Manage.* 148, 101–111.
- Giri, C., Ochieng, E., Tieszen, L.L., Zhu, Z., Singh, A., Loveland, T., Masek, J., Duke, N., 2011. Status and distribution of mangrove forests of the world using earth observation satellite data. *Global Ecol. Biogeogr.* 20, 154–159.
- Giri, C., Pengra, B., Zhu, Z., Singh, A., Tieszen, L.L., 2007. Monitoring mangrove forest dynamics of the Sundarbans in Bangladesh and India using multi-temporal satellite data from 1973 to 2000. *Estuar. Coast. Shelf Sci.* 73, 91–100.
- Giri, C., Zhu, Z., Tieszen, L.L., Singh, A., Gillette, S., Kelmelis, J.A., 2008. Mangrove forest distributions and dynamics (1975–2005) of the tsunami-affected region of Asia. *J. Biogeogr.* 35, 519–528.
- Hamilton, S.E., Casey, D., 2016. Creation of a high spatio-temporal resolution global database of continuous mangrove forest cover for the 21st century (CGMFC-21). *Global Ecol. Biogeogr.* 25, 729–738.
- Hansen, M.C., Potapov, P.V., Moore, R., Hancher, M., Turubanova, S.A., Tyukavina, A., Thau, D., Stehman, S.V., Goetz, S.J., Loveland, T.R., Kommareddy, A., Egorov, A., Chini, L., Justice, C.O., Townshend, J.R.G., 2013. High-resolution global maps of 21st-century forest cover change. *Science* 342, 850–853.
- Held, A., Ticehurst, C., Lymburner, L., Williams, N., 2003. High resolution mapping of tropical mangrove ecosystems using hyperspectral and radar remote sensing. *Int. J. Remote Sens.* 24, 2739–2759.
- Hermosilla, T., Wulder, M.A., White, J.C., Coops, N.C., Hobart, G.W., 2015. Regional detection, characterization, and attribution of annual forest change from 1984 to 2012 using Landsat-derived time-series metrics. *Remote Sens. Environ.* 170, 121–132.
- Huete, A., Didan, K., Miura, T., Rodriguez, E.P., Gao, X., Ferreira, L.G., 2002. Overview of the radiometric and biophysical performance of the MODIS vegetation indices. *Remote Sens. Environ.* 83, 195–213.
- Huete, A.R., Liu, H.Q., Batchily, K., van Leeuwen, W., 1997. A comparison of vegetation indices over a global set of TM images for EOS-MODIS. *Remote Sens. Environ.* 59, 440–451.
- Ibrahim, N.A., Mustapha, M.A., Lihan, T., Mazlan, A.G., 2015. Mapping mangrove changes in the Matang Mangrove Forest using multi temporal satellite imageries. *Ocean Coast Manage.* 114, 64–76.
- Jensen, J.R., Lin, H., Yang, X., Thoenke, C.W., 1991. The measurement of mangrove characteristics in southwest Florida using SPOT multispectral data. *Geocarto Int.* 6, 13–21.
- Jhonnerie, R., Siregar, V.P., Nababan, B., Prasetyo, L.B., Wouthuyzen, S., 2015. Random forest classification for mangrove land cover mapping using landsat 5 TM and Alos Palsar Imageries. *Procedia Environ. Sci.* 24, 215–221.
- Jia, M., Wang, Z., Li, L., Song, K., Ren, C., Liu, B., Mao, D., 2014. Mapping China's mangroves based on an object-oriented classification of Landsat imagery. *Wetlands* 34, 277–283.
- Kirui, K.B., Kairo, J.G., Bosire, J., Viergever, K.M., Rudra, S., Huxham, M., Briers, R.A., 2013. Mapping of mangrove forest land cover change along the Kenya coastline using Landsat imagery. *Ocean Coast Manage.* 83, 19–24.
- Kou, W., Xiao, X., Dong, J., Gan, S., Zhai, D., Zhang, G., Qin, Y., Li, L., 2015. Mapping deciduous rubber plantation areas and stand ages with PALSAR and landsat images. *Remote Sens.* 7, 1048–1073.
- Krause, G., Bock, M., Weiers, S., Braun, G., 2004. Mapping land-cover and mangrove structures with remote sensing techniques: a contribution to a synoptic GIS in support of coastal management in North Brazil. *Environ. Manage.* 34, 429–440.
- Lee, T., Yeh, H., 2009. Applying remote sensing techniques to monitor shifting wetland vegetation: A case study of Danshui River estuary mangrove communities, Taiwan. *Ecol Eng.* 35, 487–496.
- Li, C., Dai, H., 2014. Extraction of mangroves spatial distribution using remotely sensed data. *Wetland Sci.* 12, 580–589.
- Li, M.S., Mao, L.J., Shen, W.J., Liu, S.Q., Wei, A.S., 2013. Change and fragmentation trends of Zhanjiang mangrove forests in southern China using multi-temporal Landsat imagery (1977–2010). *Estuar. Coast. Shelf Sci.* 130, 111–120.
- Liao, B., Zhang, Q., 2014. Area, distribution and species composition of mangroves in China. *Wetland Sci.* 12, 435–440.
- Liu, K., Liu, L., Liu, H., Li, X., Wang, S., 2014. Exploring the effects of biophysical parameters on the spatial pattern of rare cold damage to mangrove forests. *Remote Sens. Environ.* 150, 20–33.
- Long, B.G., Skewes, T.D., 1996. A technique for mapping mangroves with landsat TM satellite data and geographic information system. *Estuar. Coast. Shelf Sci.* 43, 373–381.
- Long, J.B., Giri, C., 2011. Mapping the Philippines' mangrove forests using landsat imagery. *Sensors* 11, 2972–2981.
- Lü, T., Zhou, X., Liu, C., Tao, Z., Yongyut, T., 2015. Spatial distribution dataset of mangrove forests in South Asia (Mangrov_SEAsia_2015). Global Change Research Data Publishing & Repository. <<http://geodoi.ac.cn/WebCn/doi.aspx?Id=198>>.
- Maiersperger, T.K., Scaramuzza, P.L., Leigh, L., Shrestha, S., Gallo, K.P., Jenkerson, C. B., Dwyer, J.L., 2013. Characterizing LEDAPS surface reflectance products by comparisons with AERONET, field spectrometer, and MODIS data. *Remote Sens. Environ.* 136, 1–13.
- Masek, J.G., Vermote, E.F., Saleous, N., Wolfe, R., Hall, F.G., Huemmrich, F., Gao, F., Kutler, J., Lim, T.K., 2013. LEDAPS Calibration, Reflectance, Atmospheric Correction Preprocessing Code, Version 2. In.
- McCarthy, M.J., Merton, E.J., Muller-Karger, F.E., 2015. Improved coastal wetland mapping using very-high 2-meter spatial resolution imagery. *Int. J. Appl. Earth Obs.* 40, 11–18.
- McFeeters, S.K., 1996. The use of the Normalized Difference Water Index (NDWI) in the delineation of open water features. *Int. J. Remote Sens.* 17, 1425–1432.
- Nagol, J.R., Sexton, J.O., Kim, D., Anand, A., Morton, D., Vermote, E., Townshend, J.R., 2015. Bidirectional effects in Landsat reflectance estimates: Is there a problem to solve? *ISPRS J. Photogramm.* 103, 129–135.
- Nayak, S., Bahuguna, A., 2001. Application of remote sensing data to monitor mangroves and other coastal vegetation of India. *Indian Journal of Marine Sciences*. 30, 195–213.
- Olson, D.M., Dinerstein, E., Wikramanayake, E.D., Burgess, N.D., Powell, G.V.N., Underwood, E.C., D'Amico, J.A., Itoua, I., Strand, H.E., Morrison, J.C., Loucks, C.J., Allnutt, T.F., Ricketts, T.H., Kura, Y., Lamoreux, J.F., Wettenberg, W.W., Hedao, P., Kassem, K.R., 2001. Terrestrial Ecoregions of the World: A New Map of Life on Earth: A new global map of terrestrial ecoregions provides an innovative tool for conserving biodiversity. *Bioscience* 51, 933–938.
- Pattanaik, C., Narendra Prasad, S., 2011. Assessment of aquaculture impact on mangroves of Mahanadi delta (Orissa), East coast of India using remote sensing and GIS. *Ocean Coast Manage.* 54, 789–795.
- Qin, Y., Xiao, X., Dong, J., Zhang, G., Roy, P.S., Joshi, P.K., Gilani, H., Murthy, M.S., Jin, C., Wang, J., Zhang, Y., Chen, B., Menarguez, M.A., Biradar, C.M., Bajgain, R., Li, X., Dai, S., Hou, Y., Xin, F., Moore, B.R., 2016. Mapping forests in monsoon Asia with ALOS PALSAR 50-m mosaic images and MODIS imagery in 2010. *Sci. Rep.-UK* 6, 20880.

- Qin, Y., Xiao, X., Dong, J., Zhou, Y., Zhu, Z., Zhang, G., Du, G., Jin, C., Kou, W., Wang, J., Li, X., 2015. Mapping paddy rice planting area in cold temperate climate region through analysis of time series Landsat 8 (OLI), Landsat 7 (ETM+) and MODIS imagery. *ISPRS J. Photogramm.* 105, 220–233.
- Rahman, A.F., Dragoni, D., Didan, K., Barreto-Munoz, A., Hutabarat, J.A., 2013. Detecting large scale conversion of mangroves to aquaculture with change point and mixed-pixel analyses of high-fidelity MODIS data. *Remote Sens. Environ.* 130, 96–107.
- Ramírez-García, P., López-Blanco, J., Ocaña, D., 1998. Mangrove vegetation assessment in the Santiago River Mouth, Mexico, by means of supervised classification using Landsat TM imagery. *Forest Ecol Manage.* 105, 219–229.
- Reiche, J., Verbesselt, J., Hoekman, D., Herold, M., 2015. Fusing Landsat and SAR time series to detect deforestation in the tropics. *Remote Sens. Environ.* 156, 276–293.
- De Souza, Rocha, Pereira, F., Kampel, M., Cunha-Lignon, M., 2012. Mapping of mangrove forests on the southern coast of São Paulo, Brazil, using synthetic aperture radar data from ALOS/PALSAR. *Remote Sens. Lett.* 3, 567–576.
- Rodrigues, S.W.P., Souza-Filho, P.W.M., 2011. Use of multi-sensor data to identify and map tropical coastal Wetlands in the Amazon of Northern Brazil. *Wetlands* 31, 11–23.
- Rokni, K., Ahmad, A., Selamat, A., Hazini, S., 2014. Water feature extraction and change detection using multitemporal landsat imagery. *Remote Sens.* 6, 4173–4189.
- Roy, D.P., Zhang, H.K., Ju, J., Gomez-Dans, J.L., Lewis, P.E., Schaaf, C.B., Sun, Q., Li, J., Huang, H., V. K., 2016. A general method to normalize Landsat reflectance data to nadir BRDF adjusted reflectance. *Remote Sens. Environ.* 176, 255–271.
- Salami, A.T., Akinyede, J., de Gier, A., 2010. A preliminary assessment of NigeriaSat-1 for sustainable mangrove forest monitoring. *Int. J. Appl. Earth Obs.* 12, S18–S22.
- Sentinel-1 Team, 2013. Sentinel-1 User Handbook <https://sentinel.esa.int/documents/247904/685163/Sentinel-1_User_Handbook>.
- Seto, K.C., Fragkias, M., 2007. Mangrove conversion and aquaculture development in Vietnam: A remote sensing-based approach for evaluating the Ramsar Convention on Wetlands. *Global Environ. Change* 17, 486–500.
- Simard, M., Grandi, G.D., Saatchi, S., Mayaux, P., 2002. Mapping tropical coastal vegetation using JERS-1 and ERS-1 radar data with a decision tree classifier. *Int. J. Remote Sens.* 23, 1461–1474.
- Simard, M., Rivera-Monroy, V.H., Mancera-Pineda, J.E., Castañeda-Moya, E., Twilley, R.R., 2008. A systematic method for 3D mapping of mangrove forests based on Shuttle Radar Topography Mission elevation data, ICEsat/GLAS waveforms and field data: Application to Ciénaga Grande de Santa Marta, Colombia. *Remote Sens. Environ.* 112, 2131–2144.
- Spalding, M., Kainuma, M., Collins, L., 2010. World atlas of mangroves. In: *World Atlas of Mangroves*. Routledge.
- Torwick, N., Ledoux, L., Salas, W., Zhao, M., 2016. Regional mapping of plantation extent using multisensor imagery. *Remote Sens.* 8, 236.
- Tucker, C.J., 1979. Red and photographic infrared linear combinations for monitoring vegetation. *Remote Sens. Environ.* 8, 127–150.
- USGS, 2016. Provisional Landsat 8 Surface Reflectance Code (LASRC) Proudct. “Department of interior U.S. Geological Survey” <http://landsat.usgs.gov/CDR_LSR.php>.
- USGS, 2017. Landsat 4–7 Climate Data Record (CDR) Surface Reflectance. <http://landsat.usgs.gov/documents/cdr_sr_product_guide.pdf>.
- Vo, Q., Oppelt, N., Leinenkugel, P., Kuenzer, C., 2013. Remote sensing in mapping mangrove ecosystems – an object-based approach. *Remote Sens.* 5, 183–201.
- Wang, T., Zhang, H., Lin, H., Fang, C., 2016. Textural-spectral feature-based species classification of mangroves in Mai Po nature reserve from worldview-3 imagery. *Remote Sens.* 8, 24.
- Wu, P., Zhang, J., Ma, Y., Li, X., 2013. Remote sensing monitoring and analysis of the changes of mangrove resource in China in the past 20 years. *Adv. Mar. Sci.*, 406–414.
- Wu, P., Ma, Y., Li, X., Yu, G., 2011. Remote sensing monitoring of the mangrove forests resources of Guangdong Province. *J. Mar. Sci.* 29, 16–24.
- Xiao, X., Biradar, C.M., Czarnecki, C., Alabi, T., Keller, M., 2009. A simple algorithm for large-scale mapping of evergreen forests in tropical America, Africa and Asia. *Remote Sens.* 1, 355–374.
- Xiao, X., Boles, S., Frolking, S., Li, C., Babu, J.Y., Salas, W., III, B.M., 2006. Mapping paddy rice agriculture in South and Southeast Asia using multi-temporal MODIS images. *Remote Sens Environ.* 100, pp. 95–113.
- Xiao, X., Boles, S., Liu, J., Zhuang, D., Frolking, S., Li, C., Salas, W., III, B.M., 2005. Mapping paddy rice agriculture in southern China using multi-temporal MODIS images. *Remote Sens Environ.* 95, 480–492.
- Xiao, X., Zhang, Q., Braswell, B., Urbanski, S., Boles, S., Wofsy III, S., Berrien, M., Ojima, D., 2004. Modeling gross primary production of temperate deciduous broadleaf forest using satellite images and climate data. *Remote Sens. Environ.* 91, 256–270.
- Xu, H., 2006. Modification of normalised difference water index (NDWI) to enhance open water features in remotely sensed imagery. *Int. J. Remote Sens.* 27, 3025–3033.
- Zha, Y., Gao, J., Ni, S., 2003. Use of normalized difference built-up index in automatically mapping urban areas from TM imagery. *Int. J. Remote Sens.* 24, 583–594.
- Zhang, W., Chen, Z., Wang, J., 2015. Monitoring the areal variation of mangrove in Beibu Gulf coast of Guangxi China with remote sensing data. *J. Guangxi Univ. (Nat Sci Ed)*, 1570–1576.
- Zhou, Y., Xiao, X., Qin, Y., Dong, J., Zhang, G., Kou, W., Jin, C., Wang, J., Li, X., 2016. Mapping paddy rice planting area in rice-wetland coexistent areas through analysis of Landsat 8 OLI and MODIS images. *Int. J. Appl. Earth Obs.* 46, 1–12.
- Zhu, Z., Curtis, W., 2012. Object-based cloud and cloud shadow detection in Landsat imagery. *Remote Sens. Environ.* 118, 83–94.
- Zhu, Z., Wang, S., Woodcock, C.E., 2015. Improvement and expansion of the Fmask algorithm: cloud, cloud shadow, and snow detection for Landsats 4–7, 8, and Sentinel 2 images. *Remote Sens. Environ.* 159, 269–277.